REPORT 1224

EFFECTS OF WING POSITION AND FUSELAGE SIZE ON THE LOW-SPEED STATIC AND ROLLING STABILITY CHARACTERISTICS OF A DELTA-WING MODEL [1]

By Alex Goodman and David F. Thomas, Jr.

SUMMARY

An investigation was made to determine the effects of wing position and fuselage size on the low-speed static and rolling stability characteristics of airplane models having a triangular wing and vertical tail surfaces.

For the longitudinal-stability case, the results indicated that, for all wing positions, as the fuselage size was increased the maximum lift coefficient decreased. Also, for a given fuselage size, the maximum lift coefficient increased as the wing position was changed from low to high.

For the lateral-stability case, the results indicated an increase in the vertical-tail lift-curve slope as well as an increase in the effective dihedral with an increase in fuselage size. Both these effects could be calculated with good accuracy by using available theory. As indicated by both available theory and results of previous investigations, the effective dihedral at low angles of attack caused by wing-fuselage interference changed sign as the wing position was changed from low to high. Moving the wing from the low to the high position caused the vertical-tail contribution to the directional stability to decrease at low and moderate angles of attack. At high angles of attack, all the configurations investigated became directionally unstable. However, the low-wing—large-fuselage (fineness-ratio-6) configuration maintained directional stability to an angle of attack above that which corresponds to maximum lift.

For the rolling-stability case, the results generally indicated very little effect of both wing position and fuselage size.

INTRODUCTION

In recent years, the accent on high-speed flight has led to many changes in the design of the major components of airplanes. The incorporation of large amounts of sweepback in the wing and tail surfaces, use of low aspect ratio, changes in wing and horizontal-tail positions relative to the fuselage, and changes in the fuselage shape are but a few of the many changes that have led to the consideration of some configurations for which design information regarding stability characteristics is not available. In order to provide general information which would aid the designer of present-day airplanes, a series of investigations is being conducted in the Langley stability tunnel on models having various interchangeable parts. Some of these investigations have resulted in the development of methods for estimating the various stability derivatives and also have provided information with which to check the validity of existing theories. A summary of the various methods used for estimating the stability derivatives of airplanes is presented in reference 1 which contains a large number of the results obtained in the Langley stability tunnel.

The present investigation was made in order to determine the effects of wing position and fuselage size on the low-speed static and rolling stability characteristics of models having a triangular wing and vertical tail surfaces. This investigation is a continuation of the work reported in reference 2 wherein the effects of wing position on the static stability characteristics of models having unswept and 45° sweptback surfaces were obtained. The data of the present investigation have been used to determine interference effects between the wing and fuselages and between the fuselages and vertical tails and to determine the interference effects of the wing-fuselage combination on the vertical-tail contribution to the static-stability and rolling-stability parameters. Also, the lift-curve slopes of the vertical tails and the efficiency factors of the vertical tails as a function of wing position and body size have been determined. Tuft-grid pictures of the flow at the vertical tail as affected by wing-fuselage interference are also presented.

SYMBOLS

The data are presented in the form of standard NACA coefficients of forces and moments which are referred to the 25-percent-mean-aerodynamic-chord point projected on the plane of symmetry. The positive direction of the forces, moments, and angular displacements are shown as part of figure 1. The coefficients and symbols are defined as follows:

b	span, measured perpendicular to fuselage center line, ft
c	chord, measured parallel to fuselage center line, ft
$\bar{c}$	mean aerodynamic chord, $\frac{2}{S}\int_0^{b/2} c^2 dy$, ft
S	area, sq ft
x	chordwise distance from leading edge of root chord to quarter-chord point of any chord, ft
$\bar{x}$	chordwise distance from leading edge of root chord to quarter-chord point of mean aerodynamic chord, $\frac{2}{S}\int_0^{b/2} cx\, dy$, ft
y	spanwise distance measured perpendicular to fuselage center line, ft
$\bar{y}$	spanwise distance to quarter-chord point of mean aerodynamic chord, $\frac{2}{S}\int_0^{b/2} cy\, dy$, ft

[1] Supersedes NACA TN 3063, 1954.

413672—57——27

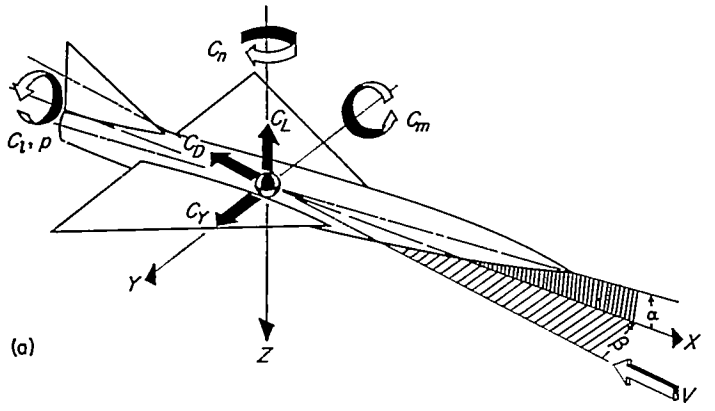

(a) Axis system.

FIGURE 1.—System of axes used and representation of flow at wing-fuselage juncture. Arrows indicate positive directions of angles, velocities, and force and moment coefficients.

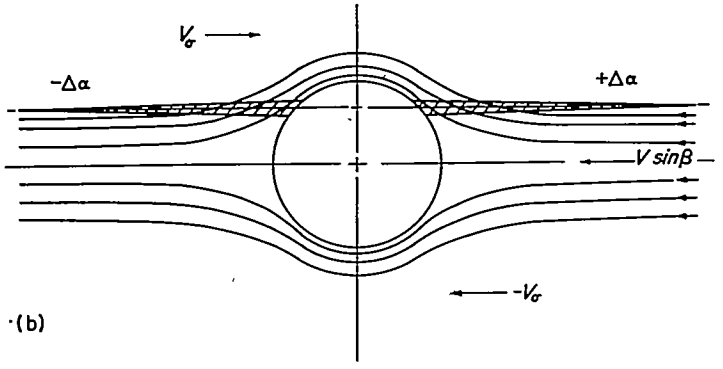

(b) Explanatory sketch for the increase in rolling moment due to sideslip by the fuselage interference and for the induced sidewash. Rear view of wing-fuselage section.

FIGURE 1.—Concluded.

z_W wing height, perpendicular distance from fuselage center line to wing chord plane (positive when wing is above fuselage center line), ft

d maximum fuselage diameter, ft

d_V diameter of fuselage at $\bar{c}/4$ of vertical tail, ft

l fuselage length, ft

S_s projected side area of fuselage, sq ft

v_F volume of fuselage, cu ft

l_V tail length, distance parallel to fuselage center line from $\bar{c}/4$ of wing to center of pressure of vertical tail, ft

z_V perpendicular distance from fuselage center line to center of pressure of vertical tail, ft

q dynamic pressure (free stream unless otherwise noted), $\frac{1}{2}\rho V^2$, lb/sq ft

ρ mass density of air, slugs/cu ft

V velocity, ft/sec

p rolling angular velocity, radians/sec

α angle of attack of wing or fuselage center line (unless otherwise noted), deg

β angle of sideslip, deg

Γ effective dihedral angle, deg

σ effective sidewash angle at vertical tail (positive when tending to make the lateral force more positive)

$\frac{\partial\sigma}{\partial\beta}$ rate of change of effective sidewash angle at vertical tail with angle of sideslip, deg/deg

η_β efficiency factor of vertical tail in sideslip

η_p efficiency factor of vertical tail in roll

$\frac{pb}{2V}$ wing-tip helix angle, radians

$\frac{\partial\sigma}{\partial\frac{pb}{2V}}$ rate of change of effective sidewash angle at vertical tail with wing-tip helix angle, radians/radian

C_L lift coefficient, $\frac{\text{Lift}}{qS_W}$

$C_{L_{max}}$ maximum lift coefficient

C_D drag coefficient, $\frac{\text{Drag}}{qS_W}$

C_Y lateral-force coefficient, $\frac{\text{Lateral force}}{qS_W}$

C_m pitching-moment coefficient, $\frac{\text{Pitching moment}}{qS_W\bar{c}_W}$

C_n yawing-moment coefficient, $\frac{\text{Yawing moment}}{qS_Wb_W}$

C_l rolling-moment coefficient, $\frac{\text{Rolling moment}}{qS_Wb_W}$

C_{Y_β} lateral-force parameter per degree, $\left(\frac{\partial C_Y}{\partial\beta}\right)_{\beta=0°}$

C_{n_β} directional-stability parameter per degree, $\left(\frac{\partial C_n}{\partial\beta}\right)_{\beta=0°}$

C_{l_β} effective-dihedral parameter per degree, $\left(\frac{\partial C_l}{\partial\beta}\right)_{\beta=0°}$

$C_{Y_{\beta V}} = -C_{L_{\alpha_V}}\frac{S_V}{S_W}$ per degree

$C_{L_{\alpha_V}}$ lift-curve slope of vertical tail (C_L of vertical tail based on vertical-tail area) per degree, $\left(\frac{\partial C_L}{\partial\alpha_V}\right)_{\alpha_V=0°}$

$C_{m_\alpha} = \left(\frac{\partial C_m}{\partial\alpha}\right)_{\alpha=0°}$ per degree

$C_{Y_p} = \frac{\partial C_Y}{\partial\frac{pb}{2V}}$ per radian

$C_{n_p} = \frac{\partial C_n}{\partial\frac{pb}{2V}}$ per radian

$C_{l_p} = \frac{\partial C_l}{\partial\frac{pb}{2V}}$ per radian

$C_{Y_{p_V}} = \frac{\partial C_{Y_V}}{\partial\frac{pb}{2V}}$ per radian

$\Delta_1C_L, \Delta_1C_m, \Delta_1C_{Y_\beta}, \Delta_1C_{n_\beta}, \Delta_1C_{l_\beta}, \Delta_1C_{Y_p}, \Delta_1C_{n_p}, \Delta_1C_{l_p}$ increments of coefficients caused by wing-fuselage interference; that is, $\Delta_1C_{Y_\beta} = C_{Y_{\beta_{W+F}}} - (C_{Y_{\beta_W}} + C_{Y_{\beta_F}})$

$\Delta_2 C_{Y_\beta}$, $\Delta_2 C_{n_\beta}$, $\Delta_2 C_{l_\beta}$, $\Delta_2 C_{Y_p}$, $\Delta_2 C_{n_p}$, $\Delta_2 C_{l_p}$ } increments of coefficients caused by wing-fuselage interference and wing interference on vertical-tail contribution; that is, $\Delta_2 C_{Y_\beta} = (C_{Y_{\beta_{W+F+V}}} - C_{Y_{\beta_{WF+F}}}) - (C_{Y_{\beta_{F+V}}} - C_{Y_{\beta_F}})$

$\Delta_3 C_{Y_\beta}$, $\Delta_3 C_{n_\beta}$, $\Delta_3 C_{l_\beta}$, $\Delta_3 C_{Y_p}$, $\Delta_3 C_{n_p}$, $\Delta_3 C_{l_p}$ } increments of coefficients caused by mutual interference of fuselage and vertical tail; that is, $\Delta_3 C_{Y_\beta} = (C_{Y_{\beta_{F+V}}} - C_{Y_{\beta_F}}) - C_{Y_{\beta_V}}$

Subscripts:

W	isolated wing
F	isolated fuselage or body
V	isolated vertical tail
WF	wing-fuselage combination
r	root
σ	component due to sidewash

APPARATUS AND MODELS

The tests of the present investigation were made in the 6-foot-diameter rolling-flow test section of the Langley stability tunnel. This section is equipped with a motor-driven rotor which may be used to impart a twist to the airstream so that a model mounted in the tunnel is in a field of flow similar to that which exists about an airplane in rolling flight (ref. 3).

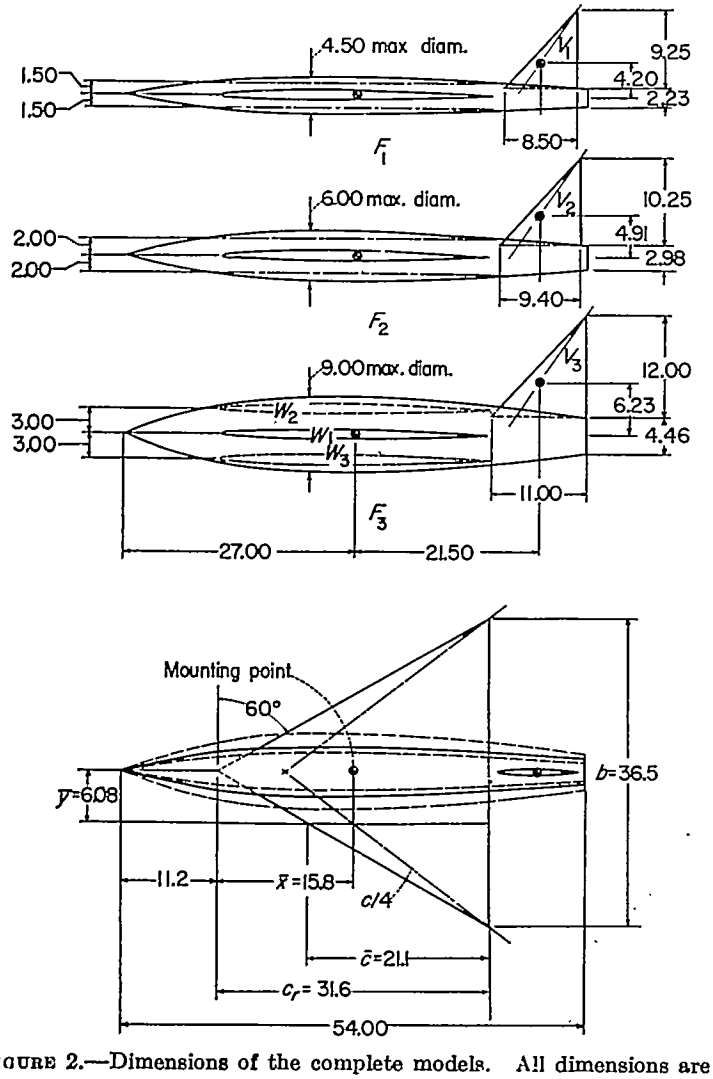

FIGURE 2.—Dimensions of the complete models. All dimensions are in inches.

Details of the wing, fuselages, and vertical tail surfaces and the relative locations of the wing and vertical tails with respect to the fuselages are given in figure 2. The various wing positions, fuselage sizes, and vertical-tail sizes will be referred to herein by the following designations:

W_1	Midwing
W_2	High wing
W_3	Low wing
F_1	Small fuselage
F_2	Medium fuselage
F_3	Large fuselage
V_1	Small vertical tail
V_2	Medium vertical tail
V_3	Large vertical tail

A list of the pertinent geometric characteristics of the various component parts is given in table I.

TABLE I.—PERTINENT GEOMETRIC CHARACTERISTICS OF MODELS

Fuselage:	F_1	F_2	F_3
Length, in.	54.0	54.0	54.0
Maximum diameter, in.	4.5	6.0	9.0
Fineness ratio	12.0	9.0	6.0
Body-size ratio, d/b_W	0.123	0.165	0.246
Volume, cu in.	545	990	2,200
Side area, sq in.	186	252	370
Wing:			
Aspect ratio			2.31
Taper ratio			0
Leading-edge sweep angle, deg			60
Dihedral angle, deg			0
Twist, deg			0
NACA airfoil section			65A003
Area, sq in.			576.7
Span, in.			36.5
Mean aerodynamic chord, in.			21.1
Root chord, in.			31.6
Wing-height ratio for all wing-fuselage combinations, z_W/d			0, ±0.333
Vertical tail:	V_1	V_2	V_3
Aspect ratio	2.18	2.18	2.18
Taper ratio	0	0	0
Leading-edge sweep angle, deg	42.5	42.5	42.5
NACA airfoil section	65–006	65–006	65–006
Area, sq in.	39.2	48.3	66.0
Span, in.	9.25	10.25	12.00
Root chord, in.	8.50	9.40	11.00
Mean aerodynamic chord, in.	5.67	6.25	7.35
Tail length, in.	21.5	21.5	21.5
Area ratio, S_V/S_W	0.068	0.084	0.115
Tail-length ratio, l_V/b_W	0.59	0.59	0.59

The complete models used for the present investigation were designed to permit tests of the wing alone, the fuselages alone, the wing-fuselage combinations (with the wing at three different vertical positions relative to the fuselage), or the fuselage in combination with any of the three vertical tails with or without the wing. The fuselages used in the investigation had fineness ratios of 6, 9, and 12 and were bodies of revolution having parabolic-arc profiles and blunt-tail ends. The wing was a 60° delta wing of aspect ratio 2.31 and had an NACA 65A003 profile in sections parallel to the plane of symmetry. All the triangular vertical tails had an aspect

ratio of 2.18, 42.5° sweepback of the leading edge, and NACA 65–006 profiles in planes parallel to the fuselage center line and differed only in area. (See table I.) Ordinates for the NACA 65A003 and 65–006 sections and for the fuselages are given in tables II and III, respectively. All parts were constructed of mahogany.

TABLE II.—ORDINATES FOR NACA 65A003 AND 65–006 AIRFOILS

[Station and ordinates in percent airfoil chord]

NACA 65A003		NACA 65–006	
Station	Ordinates	Station	Ordinates
0	0	0	0
.50	.234	.50	.476
.75	.284	.75	.574
1.25	.362	1.25	.717
2.50	.493	2.50	.956
5.00	.658	5.00	1.310
7.50	.796	7.50	1.589
10.00	.912	10.00	1.824
15.00	1.097	15.00	2.197
20.00	1.236	20.00	2.482
25.00	1.342	25.00	2.697
30.00	1.420	30.00	2.852
35.00	1.472	35.00	2.952
40.00	1.498	40.00	2.998
45.00	1.497	45.00	2.983
50.00	1.465	50.00	2.900
55.00	1.402	55.00	2.741
60.00	1.309	60.00	2.518
65.00	1.191	65.00	2.246
70.00	1.053	70.00	1.935
75.00	.897	75.00	1.594
80.00	.727	80.00	1.233
85.00	.549	85.00	.865
90.00	.369	90.00	.510
95.00	.188	95.00	.195
100.00	.007	100.00	0
L. E. radius: 0.057		L. E. radius: 0.240	

TABLE III.—FUSELAGE ORDINATES

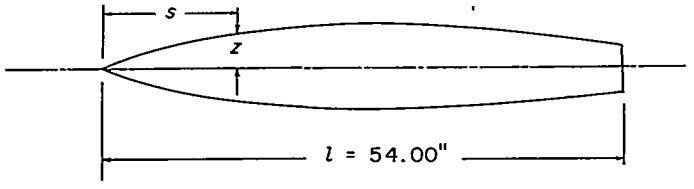

Station, s/l	Ordinate, z/l		
	F_1	F_2	F_3
0	0	0	0
.006	.0013	.0017	.0024
.009	.0019	.0024	.0037
.015	.0032	.0041	.0061
.030	.0059	.0080	.0120
.060	.0115	.0154	.0232
.090	.0167	.0222	.0333
.120	.0213	.0284	.0426
.180	.0291	.0387	.0582
.240	.0350	.0467	.0700
.300	.0391	.0520	.0780
.360	.0413	.0550	.0826
.400	.0417	.0556	.0834
.420	.0417	.0554	.0832
.480	.0413	.0552	.0826
.540	.0406	.0541	.0810
.600	.0393	.0524	.0786
.660	.0378	.0504	.0756
.720	.0357	.0476	.0713
.780	.0333	.0443	.0665
.840	.0304	.0406	.0610
.900	.0270	.0361	.0542
.960	.0233	.0313	.0469
1.000	.0208	.0276	.0413

The models were mounted on a single strut support at the quarter-chord point of the wing mean aerodynamic chord which coincided with the 50-percent point of the fuselage length (mounting point, fig. 2). Forces and moments were measured by means of a six-component balance system. The lateral force of the isolated vertical tails as well as the tails in the presence of the fuselages were obtained by means of an electrical strain gage. Photographs of two of the configurations tested are presented as figure 3. The wing was set at 0° incidence with respect to the fuselage center line in all positions.

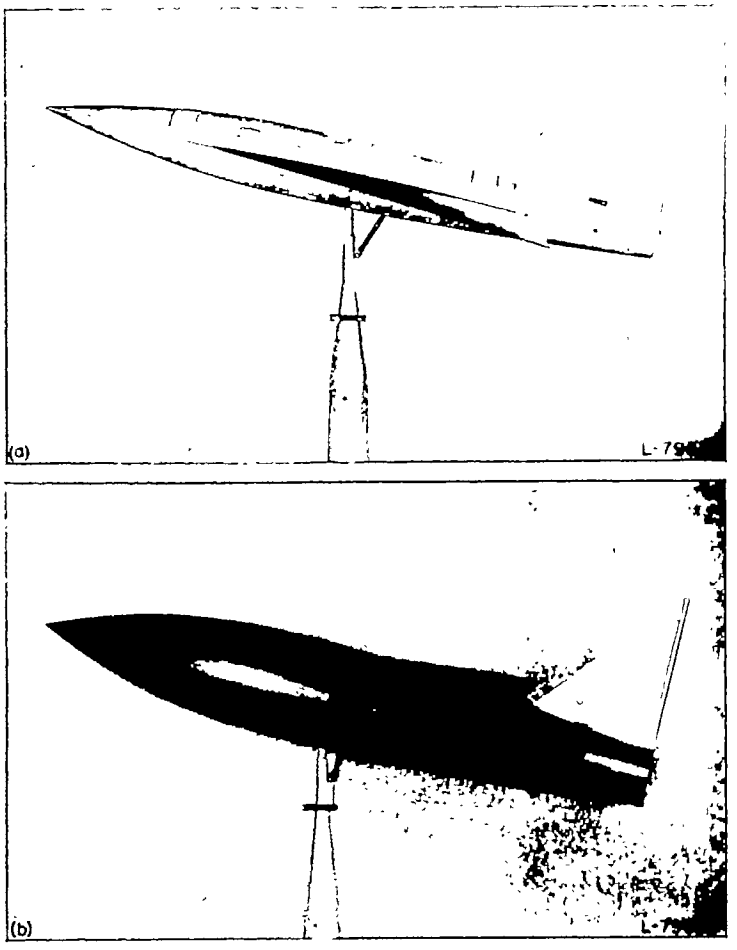

(a) Midwing, medium fuselage, and large vertical tail configuration ($W_1+F_2+V_2$).

(b) High wing, large fuselage, and large vertical tail configuration ($W_2+F_3+V_2$).

FIGURE 3.—Complete-model configurations mounted on single-strut support.

TESTS

Tests were made at a dynamic pressure of 39.8 pounds per square foot which corresponds to a Mach number of about 0.17 and a Reynolds number of 2.06×10^6 based on the mean aerodynamic chord of the wing.

The models were tested through an angle-of-attack range from about −2° up to and beyond the angle of maximum lift at angles of sideslip of 0° and ±5° in straight flow and at 0° sideslip in rolling flow. Lift, drag, and pitching moments were obtained for the straight-flow tests at 0° sideslip. Data obtained in straight flow at ±5° sideslip and in rolling flow at several values of $pb/2V$ were used to obtain the derivatives of lateral force, yawing moment, rolling moment, and lateral force on the vertical tail with respect to β and $pb/2V$. The test values of $pb/2V$ were ±0.015, ±0.030, and ±0.045.

In order to obtain the lift-curve slope of the isolated vertical tail $C_{L_{\alpha_V}}$, the tail was mounted as shown in figure 4. The angle of attack of the support system was maintained at 0° while the angle of attack of the tail was varied by pivoting the tail about the support point. The isolated tail was tested at angles of sideslip of 0° and ±5° for several angles of attack.

The tuft-grid technique of reference 4 has been used to obtain pictures of the flow at the vertical tail as affected by wing-fuselage interference. For each wing position (the large fuselage being used), pictures of the tuft grid mounted directly behind the wing-fuselage combination were obtained for zero angle of attack and for a range of sideslip angle.

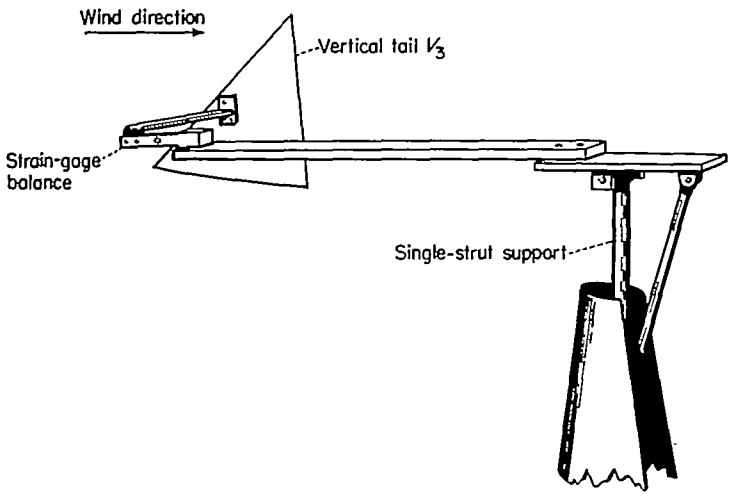

FIGURE 4.—Sketch of vertical-tail mounting for determining isolated-vertical-tail results.

CORRECTIONS

Approximate corrections, based on unswept-wing theory, for the effects of jet boundaries (ref. 5) have been applied to the angle of attack and drag coefficient. The data are not corrected for blocking, turbulence, or support-strut interference.

METHODS OF ANALYSIS

The results of the present investigation are analyzed in terms of the individual contributions of the various parts of the models to the aerodynamic characteristics and to the more important interference effects.

LONGITUDINAL-STABILITY CASE

In accordance with conventional procedures (for example, as outlined in ref. 6), the lift and pitching-moment coefficients for the present complete configurations can be expressed as

$$C_L=C_{L_W}+C_{L_F}+\Delta_1 C_L \tag{1}$$

$$C_m=C_{m_W}+C_{m_F}+\Delta_1 C_m \tag{2}$$

The increments expressed by $\Delta_1 C_L$ and $\Delta_1 C_m$ denote the mutual interference of the wing-fuselage combination. These increments can be obtained from the test results in the manner illustrated by the following equations:

$$\Delta_1 C_L=C_{L_{W+F}}-(C_{L_W}+C_{L_F}) \tag{3}$$

$$\Delta_1 C_m=C_{m_{W+F}}-(C_{m_W}+C_{m_F}) \tag{4}$$

LATERAL-STABILITY CASE

Interference increments.—By using a method analogous to the one employed for the longitudinal-stability case, the static-lateral-stability derivatives of the present complete configurations can be expressed as (see ref. 2)

$$C_{Y_\beta}=C_{Y_{\beta_W}}+C_{Y_{\beta_F}}+\Delta_1 C_{Y_\beta}+C_{Y_{\beta_V}}+\Delta_2 C_{Y_\beta}+\Delta_3 C_{Y_\beta} \tag{5}$$

The interference increments can be obtained from the test results in a manner analogous to that used for the longitudinal-stability case. For example:

$$\Delta_1 C_{Y_\beta}=C_{Y_{\beta_{W+F}}}-(C_{Y_{\beta_W}}+C_{Y_{\beta_F}}) \tag{6}$$

$$\Delta_2 C_{Y_\beta}=(C_{Y_{\beta_{W+F+V}}}-C_{Y_{\beta_{W+F}}})-(C_{Y_{\beta_{F+V}}}-C_{Y_{\beta_F}}) \tag{7}$$

$$\Delta_3 C_{Y_\beta}=(C_{Y_{\beta_{F+V}}}-C_{Y_{\beta_F}})-C_{Y_{\beta_V}} \tag{8}$$

The mutual interference increments of the fuselage—vertical-tail combination, that is, $\Delta_3 C_{Y_\beta}$, $\Delta_3 C_{n_\beta}$, and $\Delta_3 C_{l_\beta}$, are made up of two separate interference increments. For example, the increment $\Delta_3 C_{Y_\beta}$ is made up of the interference of the fuselage on the vertical tail, which can be expressed as

$$\Delta_4 C_{Y_\beta}=(C_{Y_{\beta_V}})_F-C_{Y_{\beta_V}} \tag{9}$$

and the interference of the vertical tail on the fuselage

$$\Delta_5 C_{Y_\beta}=(C_{Y_{\beta_{F+V}}}-C_{Y_{\beta_F}})-(C_{Y_{\beta_V}})_F \tag{10}$$

where $(C_{Y_{\beta_V}})_F$ is the vertical-tail contribution to C_{Y_β} in the presence of the fuselage. Equations (9) and (10) when added together result in equation (8).

Vertical-tail efficiency factors.—The vertical-tail contribution to the lateral-stability derivatives as affected by the wing-fuselage interference can, for example, be expressed as

$$(C_{Y_{\beta_V}})_{WF}=-C_{L_{\alpha_V}}\frac{S_V}{S_W}\left[\left(1-\frac{\partial\sigma}{\partial\beta}\right)\frac{q_V}{q}\right]_{WF}$$

$$=C_{Y_{\beta_V}}\left[\left(1-\frac{\partial\sigma}{\partial\beta}\right)\frac{q_V}{q}\right]_{WF} \tag{11}$$

where $(C_{Y_{\beta_V}})_{WF}$ is the vertical-tail contribution to C_{Y_β} in the presence of the wing-fuselage combination. Similarly, the contribution of the vertical tail to C_{Y_β} as affected by the fuselage interference can be expressed as

$$(C_{Y_{\beta_V}})_F=C_{Y_{\beta_V}}\left[\left(1-\frac{\partial\sigma}{\partial\beta}\right)\frac{q_V}{q}\right]_F \tag{12}$$

Solving equations (11) and (12) for the efficiency factors gives, for wing-fuselage interference,

$$(\eta_\beta)_{WF}=\left[\left(1-\frac{\partial\sigma}{\partial\beta}\right)\frac{q_V}{q}\right]_{WF}=\frac{(C_{Y_{\beta_V}})_{WF}}{C_{Y_{\beta_V}}} \tag{13}$$

and, for fuselage interference,

$$(\eta_\beta)_F=\left[\left(1-\frac{\partial\sigma}{\partial\beta}\right)\frac{q_V}{q}\right]_F=\frac{(C_{Y_{\beta_V}})_F}{C_{Y_{\beta_V}}} \tag{14}$$

ROLLING-STABILITY CASE

Interference increments.—In a manner similar to the lateral-stability case, the rolling derivatives of the present complete configuration can be expressed as

$$C_{Y_p}=C_{Y_{p_W}}+C_{Y_{p_F}}+\Delta_1 C_{Y_p}+C_{Y_{p_V}}+\Delta_2 C_{Y_p}+\Delta_3 C_{Y_p} \quad (15)$$

The interference increments can be obtained from the test results in a manner analogous to that used for the lateral-stability case. For example,

$$\Delta_1 C_{Y_p}=C_{Y_{p_{W+F}}}-\left(C_{Y_{p_W}}+C_{Y_{p_F}}\right) \quad (16)$$

$$\Delta_2 C_{Y_p}=\left(C_{Y_{p_{W+F+V}}}-C_{Y_{p_{W+F}}}\right)-\left(C_{Y_{p_{F+V}}}-C_{Y_{p_F}}\right) \quad (17)$$

The mutual interference increments of the fuselage—vertical-tail combination $\Delta_3 C_{Y_p}$, $\Delta_3 C_{n_p}$, and $\Delta_3 C_{l_p}$ are not evaluated, because values of the rolling-stability derivatives of the isolated vertical tail were not obtained.

Vertical-tail efficiency factor.—In accordance with the development of reference 7, the vertical-tail contribution to the rolling-stability derivatives as affected by the wing-gefusela interference can, for example, be expressed as

$$\left(C_{Y_{p_V}}\right)_{WF}=-57.3C_{Y_{\beta_V}}\left[-\frac{2}{b}(z_V\cos\alpha-l_V\sin\alpha)+\frac{\partial\sigma}{\partial\frac{pb}{2V}}\right]_{WF}\frac{q_V}{q} \quad (18)$$

where $\left(C_{Y_{p_V}}\right)_{WF}$ is the vertical-tail contribution to C_{Y_p} in the presence of the wing-fuselage combination.

Similarly, the contribution of the vertical tail to C_{Y_p} as affected by the fuselage interference can be expressed as

$$\left(C_{Y_{p_V}}\right)_{F}=-57.3C_{Y_{\beta_V}}\left[-\frac{2}{b}(z_V\cos\alpha-l_V\sin\alpha)+\frac{\partial\sigma}{\partial\frac{pb}{2V}}\right]_{F}\frac{q_V}{q} \quad (19)$$

Solving equations (18) and (19) for the efficiency factors gives, for wing-fuselage interference,

$$(\eta_p)_{WF}=-\frac{\left(C_{Y_{p_V}}\right)_{WF}}{57.3C_{Y_{\beta_V}}}=\left[-\frac{2}{b}(z_V\cos\alpha-l_V\sin\alpha)+\frac{\partial\sigma}{\partial\frac{pb}{2V}}\right]_{WF}\frac{q_V}{q} \quad (20)$$

and, for fuselage interference,

$$\eta_p)_F=-\frac{\left(C_{Y_{p_V}}\right)_F}{57.3C_{Y_{\beta_V}}}=\left[-\frac{2}{b}(z_V\cos\alpha-l_V\sin\alpha)+\frac{\partial\sigma}{\partial\frac{pb}{2V}}\right]_{F}\frac{q_V}{q} \quad (21)$$

RESULTS AND DISCUSSION

PRESENTATION OF RESULTS

The results for the configurations investigated are presented in three parts. The static longitudinal stability characteristics are given in figures 5 to 11 and the static lateral stability characteristics are presented in figures 12 to 28. The rolling stability characteristics are presented in figures 29 to 38.

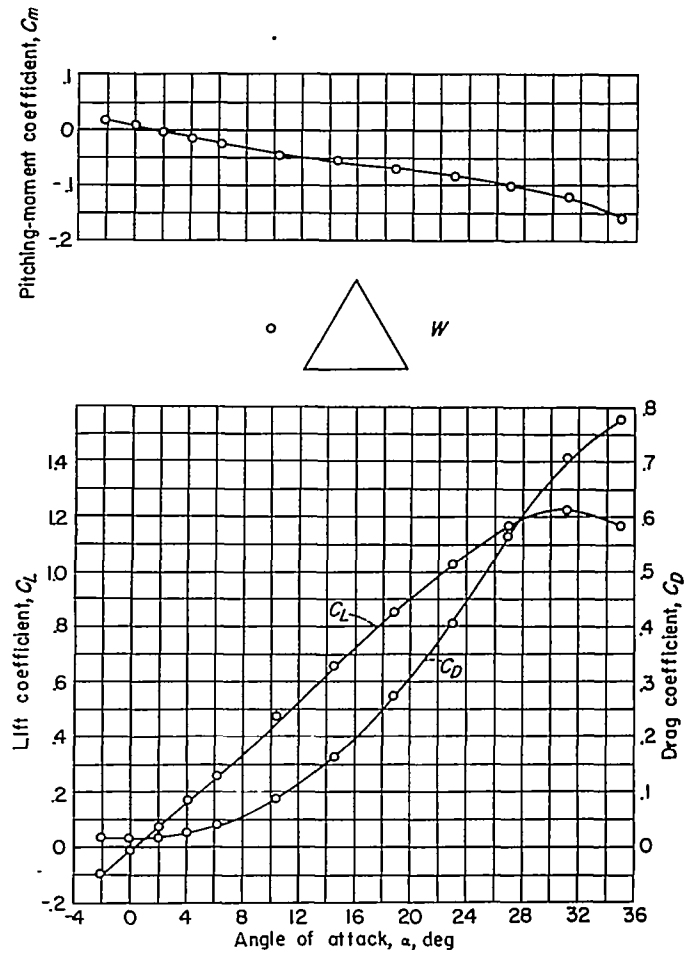

FIGURE 5.—Aerodynamic characteristics of the 60° delta wing.

STATIC LONGITUDINAL STABILITY CHARACTERISTICS

Wing characteristics.—The lift, drag, and pitching-moment data for the 60° delta wing of the present investigation are presented in figure 5. The value of the experimental lift-curve slope, taken through zero angle of attack, of 0.043 is in close agreement with the theoretical value of 0.042 given in reference 8. At low angles of attack, the aerodynamic center of the wing is located at about 37 percent of the mean aerodynamic chord. The theoretical value of 33 percent given in reference 8 is in fair agreement with this experimental value.

Fuselage and fuselage—vertical-tail characteristics.—One of the main effects of the isolated fuselage on the static longitudinal stability is the contribution of an unstable pitching moment as shown in figure 6. The unstable pitching moment at low angles of attack increases with an increase in fuselage size. This effect is in agreement with the theory of reference 9 and the results of reference 10. However, the instability in pitch decreases as the angle of attack increases for these blunt-tail fuselages.

The addition of a vertical tail to the fuselages generally had a small effect on the longitudinal stability characteristics. The validity of the lift results obtained for configuration F_3+V_3 is questionable.

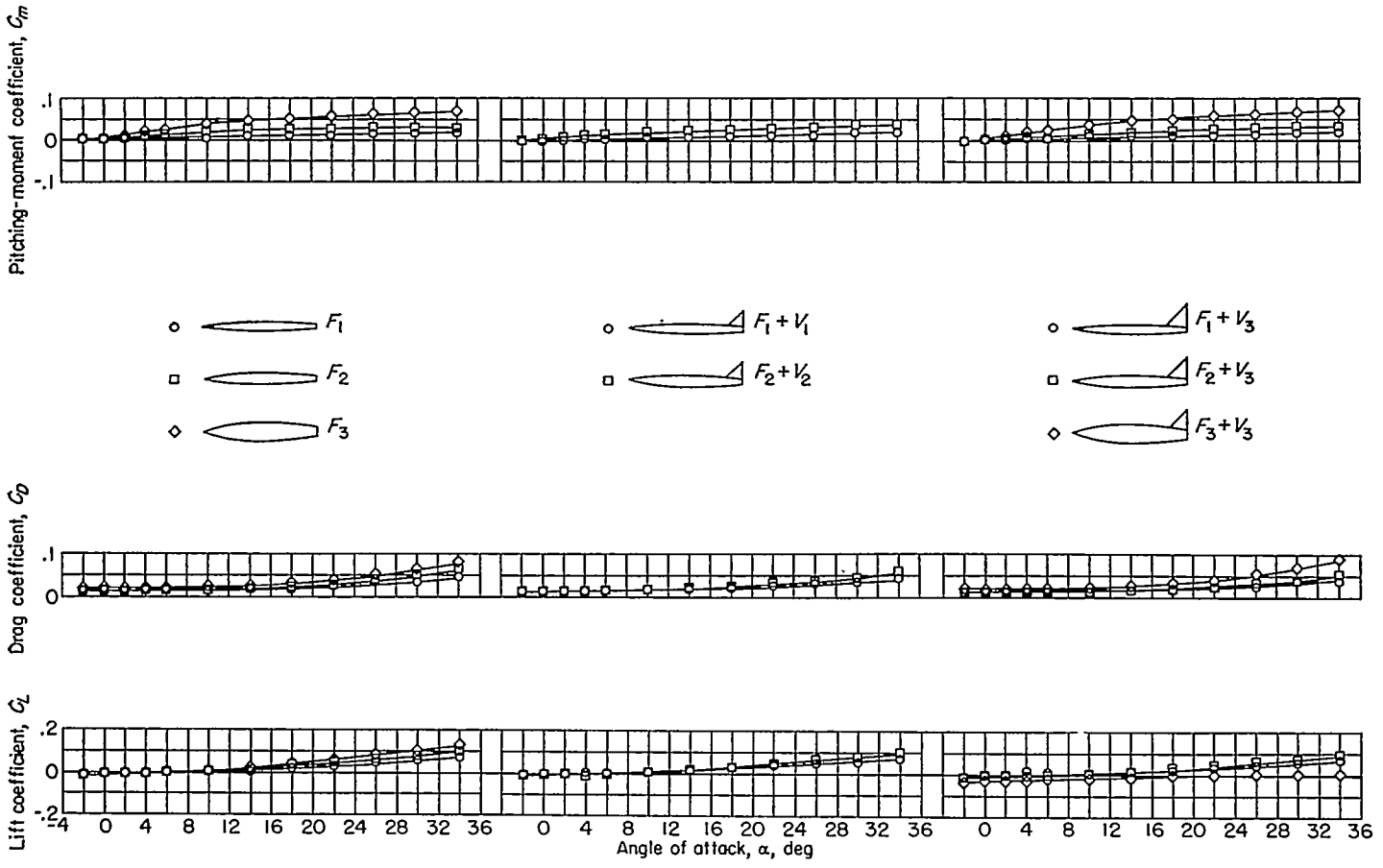

FIGURE 6.—Aerodynamic characteristics of the fuselages and the fuselages in combination with several vertical tails.

Wing-fuselage and complete-model characteristics.—The addition of a 60° delta wing in the low, middle, and high positions (W_3, W_1, or W_2, respectively) to the fuselages (F_1, F_2, or F_3) produced C_{m_α} characteristics at low angles of attack similar to that obtained for the wing alone. (Compare fig. 5 with fig. 7.) At moderate and high angles of attack, all the configurations tested exhibited stable pitching characteristics with the exception of the low-wing—large-fuselage configuration W_3+F_3. In this case, an instability is indicated at $\alpha \approx 24°$. This angle of attack also corresponds to the angle of attack at which $C_{L_{max}}$ occurs and to a break in the drag curve for this configuration. As the fuselage size is decreased, $C_{L_{max}}$ is increased and the tendency for instability is delayed to a higher angle of attack. These effects can probably be accounted for by consideration of the interaction of the delta-wing vortex with the fuselage and the wing-fuselage interference effects ($\Delta_1 C_m$ and $\Delta_1 C_L$) as shown in figure 8. As can be seen, the slope $\frac{\partial(\Delta_1 C_m)}{\partial \alpha}$ increased as the fuselage size was increased. The increment $\Delta_1 C_L$ also increases with an increase in fuselage size; however, the increase becomes less as the wing is moved from the low to the high positions. The interference is, therefore, a function of the body-size ratio and decreases with a decrease in the ratio. The variation of $C_{L_{max}}$ with body-size ratio and wing-height ratio is presented in figure 9 and illustrates this effect. Also, as can be seen in figure 9, the high-wing configurations attained the highest $C_{L_{max}}$.

The addition of a vertical tail to the wing-fuselage combinations had little effect on the longitudinal stability characteristics. (Compare figs. 10 and 11 with fig. 7.)

STATIC LATERAL STABILITY CHARACTERISTICS

Wing characteristics.—The variations of C_{Y_β}, C_{n_β}, and C_{l_β} with angle of attack for the 60° delta wing are presented in figure 12. The derivative C_{Y_β} and C_{n_β} are generally small for most of the angle-of-attack range. The value of the slope $\partial C_{l_\beta}/\partial C_L$ through $\alpha=0°$ of 0.0047 for this wing is in good agreement with the value of 0.0050 calculated by the method of reference 11.

Fuselage characteristics.—The main contribution of the isolated fuselages to the static lateral stability characteristics is an unstable yawing moment throughout the angle-of-attack range (see fig. 13). The magnitude of the unstable yawing moment at low angles of attack is apparently a direct function of the fuselage size. The fuselage characteristics at $\alpha=0°$ are summarized in figure 14. In order that the results obtained may be applied conveniently to arbitrary airplane configurations, coefficients in terms of fuselage dimensions are needed. This end is accomplished by plotting the quantities $(C_{Y_\beta})_F \frac{S_W}{S_s}$ and $(C_{n_\beta})_F \frac{S_W b_W}{v_F}$ against fuselage fineness ratio. The quantities plotted, therefore, are effectively a lateral-force coefficient based on fuselage side area S_s and a yawing-moment coefficient based on fuselage volume v_F.

The results presented in figure 14 are compared with the results of reference 12 and the theory of references 9 and 13.

The experimental results show a negative lateral force which increases as the fineness ratio is decreased; this result is in good agreement with the results of reference 12. The theory of reference 9, which is based on potential-flow consideration for closed bodies, predicts no lateral force. The theory of reference 13 results in a fair estimation of the fuselage lateral-force coefficient. The experimental results obtained for the directional-stability parameter $(C_{n_\beta})_F$ show good agreement with the results of reference 12 and are in fair agreement with the theories of references 9 and 13.

Fuselage-tail characteristics.—The addition of a vertical tail to the fuselages contributes a stable yawing moment and an increase in lateral force. However, the magnitude of the tail contribution to both C_{Y_β} and C_{n_β} is apparently a function of the ratio of the fuselage diameter (measured in the plane of the tail $\bar{c}/4$) to tail span (d_V/b_V). (See fig. 13.) Results obtained by measurement of the lift on the tail in the presence of each fuselage through the angle-of-attack range are presented in figure 15 as $\left(C_{Y_{\beta_V}}\right)_F$ where $\left(C_{Y_{\beta_V}}\right)_F$ is the vertical-tail lift-curve slope based on the wing area. The variation of the efficiency factor $(\eta_\beta)_F$ as determined by the procedures explained in the section entitled "Methods of Analysis" is presented in figure 16 with angle of attack. This factor is a direct measure of the induced sidewash at the tail for $\alpha=0°$. The effects of fuselage size on the efficiency factor $(\eta_\beta)_F$ and the tail lift-curve slope $C_{L_{\alpha_V}}$ (based on tail area) are summarized in figure 17 for $\alpha=0°$ and show an increase in $(\eta_\beta)_F$ and $C_{L_{\alpha_V}}$ as the fuselage diameter is increased. The effect of fuselage size could be calculated with good accuracy by using a finite-step method such as discussed in reference 14 and by accounting for the effects of the fuselage by using a method similar to that of reference 15. This method also yields the span loading on the tail. The calculated values are also in good agreement with the experimental results and indicate an increase in stabilizing sidewash at the vertical tail with an increase in fuselage size. (See fig. 15.)

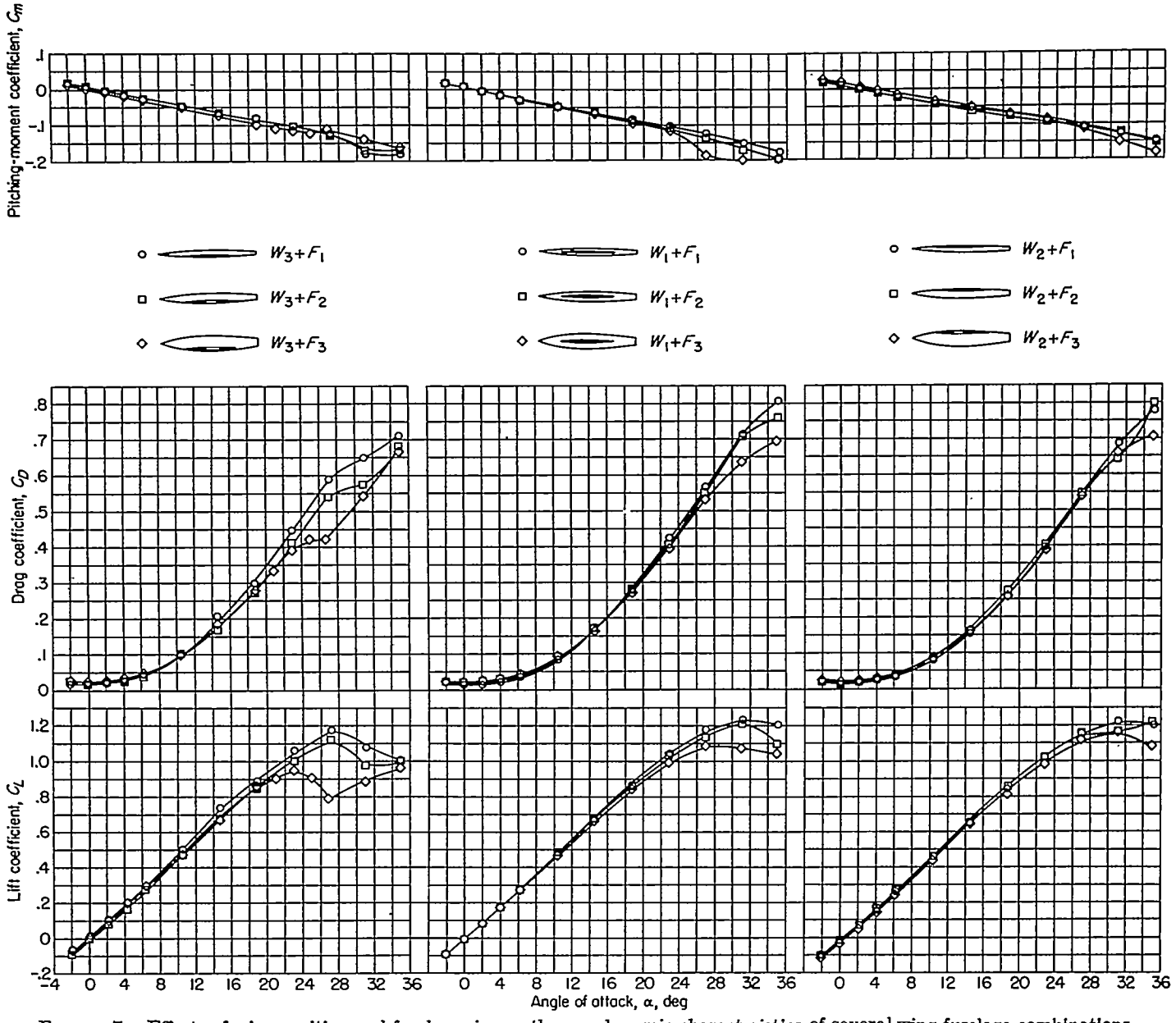

FIGURE 7.—Effects of wing position and fuselage size on the aerodynamic characteristics of several wing-fuselage combinations.

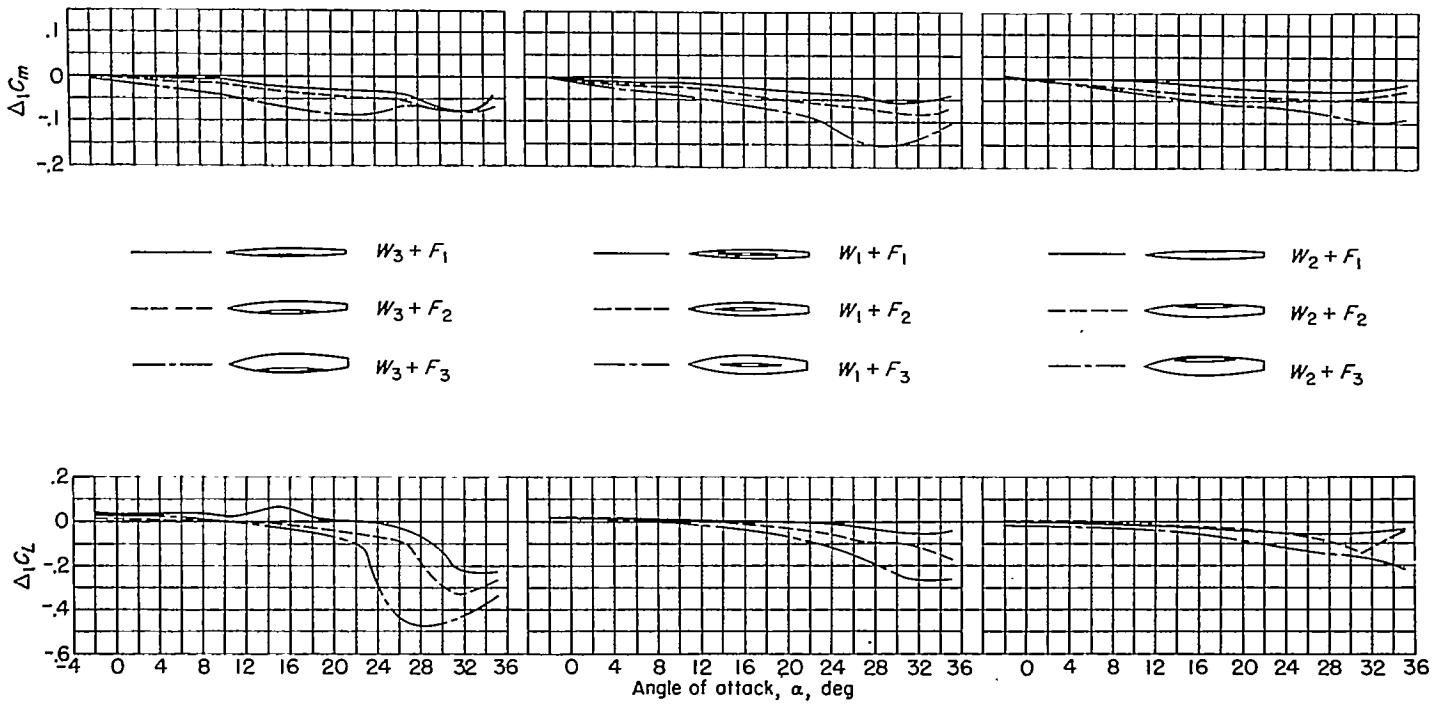

FIGURE 8.—Effects of wing position and fuselage size on the wing-fuselage interference increments $\Delta_1 C_m$ and $\Delta_1 C_L$ for the wing-fuselage combinations.

The variation of the isolated-vertical-tail lift-curve slope with angle of attack of the model is presented in figure 18. As shown the effects of angle of attack are small and the values of $C_{L_{\alpha_V}}$ could be calculated with good accuracy by using a finite-step method. The isolated-tail results were used mainly for calculating the mutual interference increment of the fuselage-tail combination $\Delta_3 C_{Y_\beta}$. These results are presented in figure 19. As indicated by the procedure outlined in the section entitled "Methods of Analysis," the mutual interference increment $\Delta_3 C_{Y_\beta}$ is composed of the interference of the fuselage on the vertical tail $\Delta_4 C_{Y_\beta}$ and the interference of the tail on the fuselage $\Delta_5 C_{Y_\beta}$. It is of importance to note here that the interference increments $\Delta_4 C_{Y_\beta}$ and $\Delta_5 C_{Y_\beta}$ are of the same magnitude at $\alpha=0°$ for practically all the configurations investigated. A similar result was obtained for upswept tail-fuselage configurations as indicated in reference 16. The present results as well as the results of reference 16 indicate that the load induced on the vertical tail by the fuselage is equal to the load induced on the fuselage by the vertical tail. As mentioned previously, the contribution to C_{Y_β} of the tail alone as well as the tail in the presence of the fuselage can be calculated with good accuracy. The results obtained, therefore, indicated a simple means of estimating the values of C_{Y_β} of the fuselage-tail combination at $\alpha=0°$.

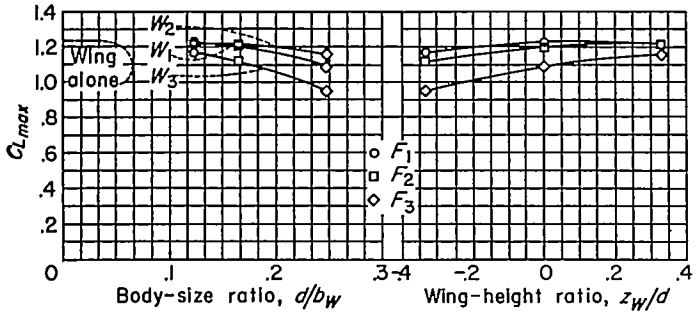

FIGURE 9.—Variation of $C_{L_{max}}$ with body-size ratio and wing-height ratio.

Wing-fuselage characteristics.—The wing-fuselage characteristics are presented in figure 20. The effects of wing position on C_{Y_β} and C_{l_β} for a given fuselage size at low angles of attack for these models are very similar to those effects obtained for the unswept and swept-back wing models discussed in reference 2. The qualitative analysis of references 2 and 17 used to account for the effects of wing position on C_{Y_β} and C_{l_β} can also be applied to the present case. Briefly, this analysis states that for a high-wing—fuselage configuration at a positive angle of sideslip the lateral component of the free-stream velocity ($V \sin \beta$) will give rise to an antisymmetrical variation in angle of attack; that is, the flow about the fuselage induces an upwash on the advancing wing semispan and a downwash on the opposite semispan. (See fig. 1 (b).) The magnitude of these induced velocities is a function of the fuselage size and can be calculated from flow considerations about an infinite cylinder (ref. 18). It can be seen, therefore, that for positive sideslip angles a negative rolling moment will be induced and that for a midwing configuration this effect does not exist. In addition, at low angles of attack, a high-wing or low-wing configuration at an angle of sideslip should have larger values of C_{Y_β} relative to the midwing results because of the end-plate effect of the wing. The results for C_{l_β} and C_{Y_β} shown in figure 20 are in agreement, at low angles of attack, with the preceding analysis.

The wing-fuselage configurations are directionally unstable throughout the angle-of-attack range investigated (fig. 20). The unstable yawing moment of the fuselages predominates

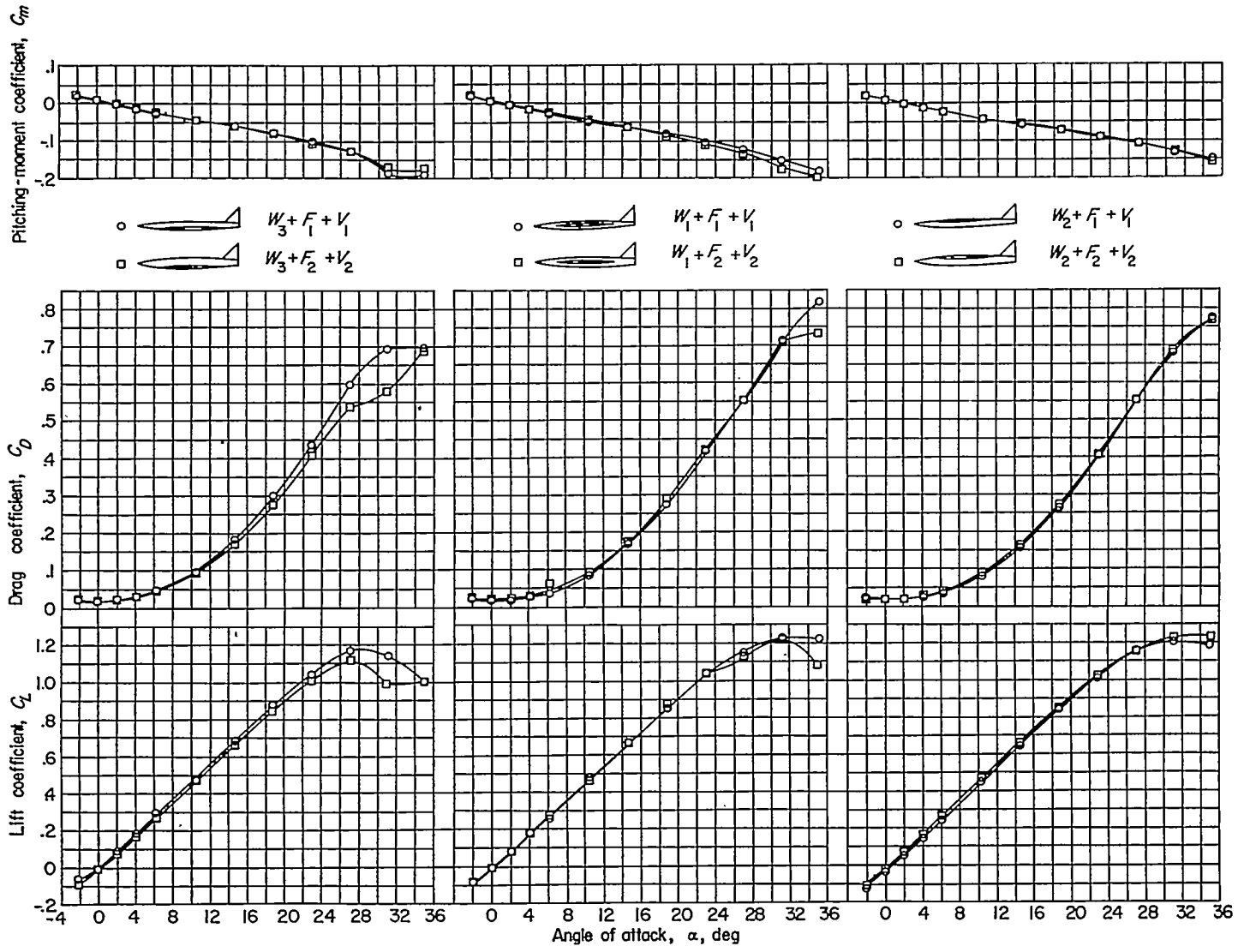

FIGURE 10.—Effects of wing position and fuselage size on the aerodynamic characteristics of several wing—fuselage—vertical-tail configurations. Small and medium vertical tails V_1 and V_2.

for the low and moderate angle-of-attack range. (Compare fig. 13 with fig. 20.) At high angles of attack, the wing-fuselage configurations became more directionally unstable; however, the increase in directional instability is less for the high-wing configurations than for the midwing or low-wing configurations.

As pointed out in the section entitled "Static Longitudinal Stability Characteristics," the low-wing—large-fuselage configuration W_3+F_3 exhibited breaks in the curves of C_L, C_D, and C_m against angle of attack at $\alpha \approx 24°$. Similar breaks are exhibited by the derivatives C_{Y_β}, C_{n_β}, and C_{l_β} at about the same angle of attack.

The wing-fuselage interference increments $\Delta_1 C_{Y_\beta}$, $\Delta_1 C_{n_\beta}$, and $\Delta_1 C_{l_\beta}$ determined by the procedures explained in the section entitled "Methods of Analysis" are presented in figure 21. In accordance with the qualitative analysis of references 2 and 17 which has been restated briefly herein, it can be seen that the wing-fuselage interference induces a negative increment of rolling moment for the high-wing configurations and a positive increment for the low-wing configurations at low angles of attack. These increments increase with an increase in fuselage size. For the midwing configurations, the interference increments $\Delta_1 C_{l_\beta}$ are about zero at $\alpha=0°$ and small at low and moderate angles of attack. The effects of fuselage size and wing position on the increment $\Delta_1 C_{l_\beta}$ at $\alpha=0°$ are presented in figure 22. The results are compared with values given by the empirical relation of reference 1 and values calculated by using a procedure similar to that of reference 15. In general, both procedures result in good agreement. However, the results obtained by using the finite-step method also yield the antisymmetrical span load distribution on the wing. In general the effective dihedral ($C_{l_\beta}/\Gamma=-0.00012$ from ref. 11) varied from approximately $\pm 2°$ to $\pm 8°$ as the fuselage size was increased. The effects of wing position are similar to the results presented in references 2 and 17.

As shown in figure 21, the interference increment $\Delta_1 C_{Y_\beta}$ is negative at low angles of attack for both the high-wing and the low-wing configurations. This increment also increases with an increase in fuselage size. At high angles of attack, $\Delta_1 C_{Y_\beta}$ attains large positive values for the low-wing configuration, whereas, for the high-wing configura-

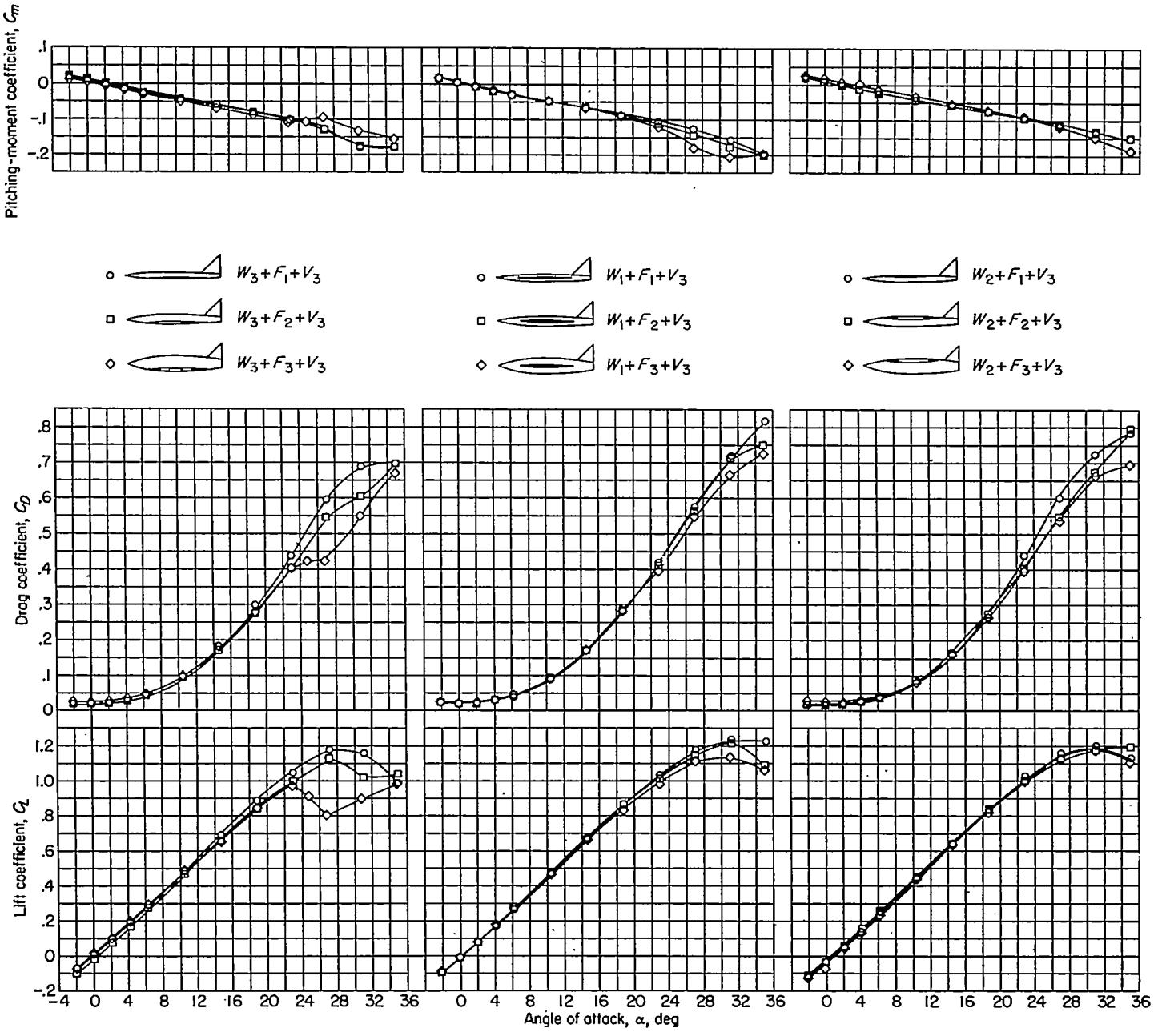

FIGURE 11.—Effects of wing position and fuselage size on the aerodynamic characteristics of several wing—fuselage—vertical-tail configurations. Large vertical tail V_3.

tion, this interference increment tends to remain negative or becomes slightly positive. These variations with angle of attack can probably be attributed to the effects of the induced sidewash on the fuselage (see refs. 2 and 17).

The interference increment $\Delta_1 C_{n_\beta}$ is small over the low and moderate angle-of-attack range for all the configurations investigated. At the high angles of attack this increment indicates an increase in directional instability for all the configurations; however, the increase in directional instability is less for the high-wing configurations than for the midwing or low-wing configurations.

Complete-model characteristics.—The qualitative analysis of the effects of wing-fuselage interference given in the preceding section entitled "Wing-fuselage characteristics" will be extended to include the effects of wing-fuselage interference on the vertical-tail contribution. As pointed out in the preceding analysis, the lateral flow about the fuselage induces an antisymmetrical lift distribution over the wing. Actually, this variation in lift caused by the fuselage is largely concentrated over a small region at the center of the wing as indicated in references 17 and 19. In this region, a large spanwise pressure gradient is produced on the wing (ref. 17) which will induce sidewash at the tail as illustrated in figure 1(b) and by the tuft-grid studies shown in figure 23. The tuft-grid results of figure 23 indicate that, for a low-wing configuration at $\alpha=0°$, the sidewash at the tail is favorable (increase in directional stability); whereas, for the high-wing configuration, the sidewash reverses sign and becomes unfavorable (decrease in directional stability). For the midwing configuration, a favorable sidewash is also indicated although theoretically it is zero (ref. 17). The sidewash velocity produced by sideslip is proportional to the angles of

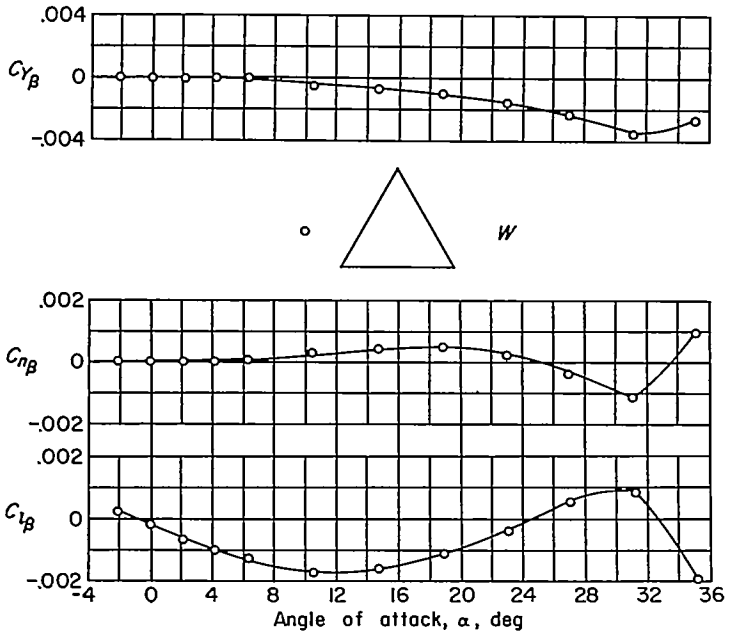

FIGURE 12.—Static lateral stability characteristics of the 60° delta wing.

sideslip and also fuselage size and is theoretically independent of the angle of attack. However, because the position of the tail relative to the center of the wing wake changes with angle of attack, the effect of the sidewash on the tail contribution will also vary with angle of attack since, in passing through the wing wake, the sidewash changes direction.

The results presented in figures 15, 24, and 25 are in agreement with preceding analysis. As indicated in figure 25 changing the wing from the low to the high position produces a large decrease in the directional-stability parameter C_{n_β} at low or moderate angles of attack. This decrease is directly related to the decrease in the tail contribution $(C_{Y_{\beta_V}})_{WF}$ with change in the wing from the low to the high position as shown in figure 15. It should be noted that C_{n_β} also decreases with an increase in fuselage size at low and moderate angles of attack for all the configurations investigated. This decrease, however, is mainly due to the increase in the unstable yawing-moment contribution of the fuselage as the fuselage size is increased. (See figs. 13 and 20.)

At high angles of attack all the configurations investigated are directionally unstable. However, the configuration with the low wing, the large fuselage, and the large vertical tail ($W_3+F_3+V_3$) maintains its directional stability to an angle of attack above that which corresponds to $C_{L_{max}}$. The other low-wing and midwing configurations become directionally unstable at angles of attack which correspond to $C_{L_{max}}$. In the case of the high-wing configurations, directional instability is attained at angles of attack which correspond to values below $C_{L_{max}}$. (See fig. 25.) The variations of the tail contribution $(C_{Y_{\beta_V}})_{WF}$ at high angles of attack also indicate these trends. (See fig. 15.)

The increments of wing-fuselage interference on the vertical-tail contributions $\Delta_2 C_{Y_\beta}$, $\Delta_2 C_{n_\beta}$, and $\Delta_2 C_{l_\beta}$ were evaluated from the basic data by the procedure outlined in the section entitled "Methods of Analysis." These increments are presented in figures 26 and 27 and the efficiency factor $(\eta_\beta)_{WF}$ presented in figure 28 is used in order to summarize these results since this factor is a direct measure of the effects of the wing-fuselage interference on the tail. At low angles of attack (fig. 28) for a given fuselage size the efficiency factor decreases as the wing-height ratio is increased from negative to positive. This effect, as mentioned previously, is mainly due to the change in the induced sidewash. As the body-size ratio is increased the efficiency factor increases for the low-wing configuration and decreases for the

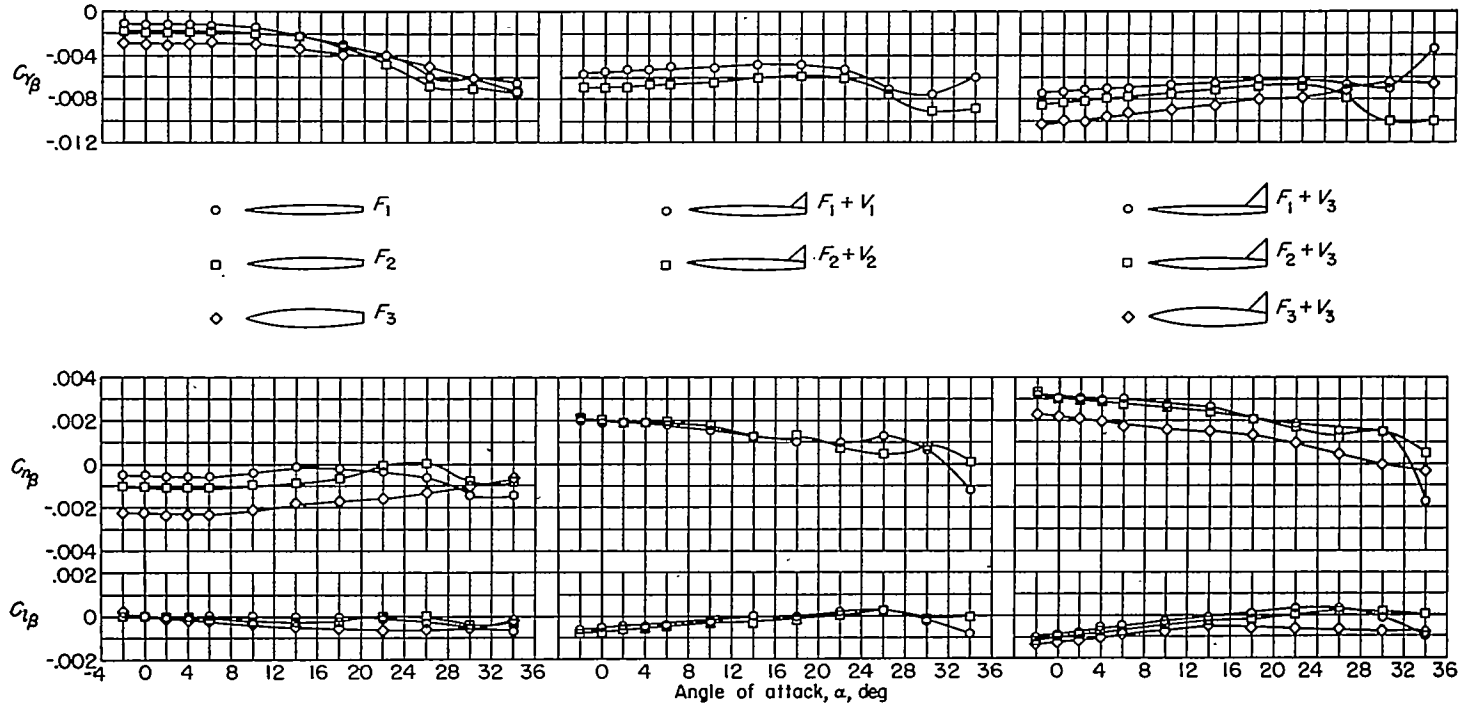

FIGURE 13.—Static lateral stability characteristics of the fuselages and the fuselages in combination with several vertical tails.

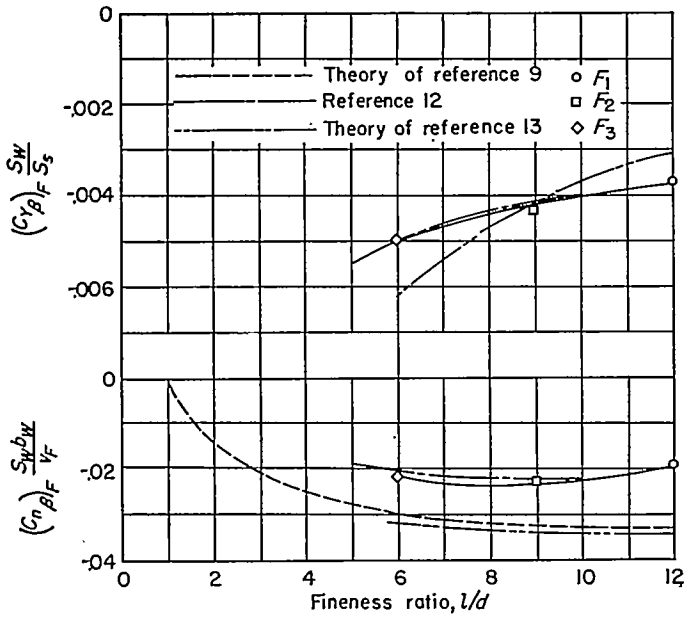

FIGURE 14.—Summary of fuselage contributions to C_{Y_β} and C_{n_β}. $\alpha = 0°$.

high-wing configuration. This effect is due to an increase in the induced sidewash with an increase in fuselage size. For the midwing configuration there is very little effect of fuselage size (fig. 28). At high angles of attack the efficiency factor of the vertical tail decreases for all the configurations investigated (see fig. 16). A large portion of this reduction in the efficiency factor may be attributed to the effects of the inboard movement of the delta-wing vortices (see ref. 4).

ROLLING STABILITY CHARACTERISTICS

Wing characteristics.—The rolling stability derivatives for the wing alone are presented in figure 29. In general, the derivatives C_{Y_p} and C_{n_p} are small over the low and moderate angle-of-attack range. The value of C_{l_p} of -0.16 at low angles of attack obtained for this wing is in excellent agreement with the theoretical value given in reference 20. At high angles of attack, C_{n_p} becomes more positive and attains a value of 0.20 at $C_{L_{max}}$. Also C_{l_p} becomes more negative (increase in damping) at high angles of attack and attains a value of -0.27 at $C_{L_{max}}$.

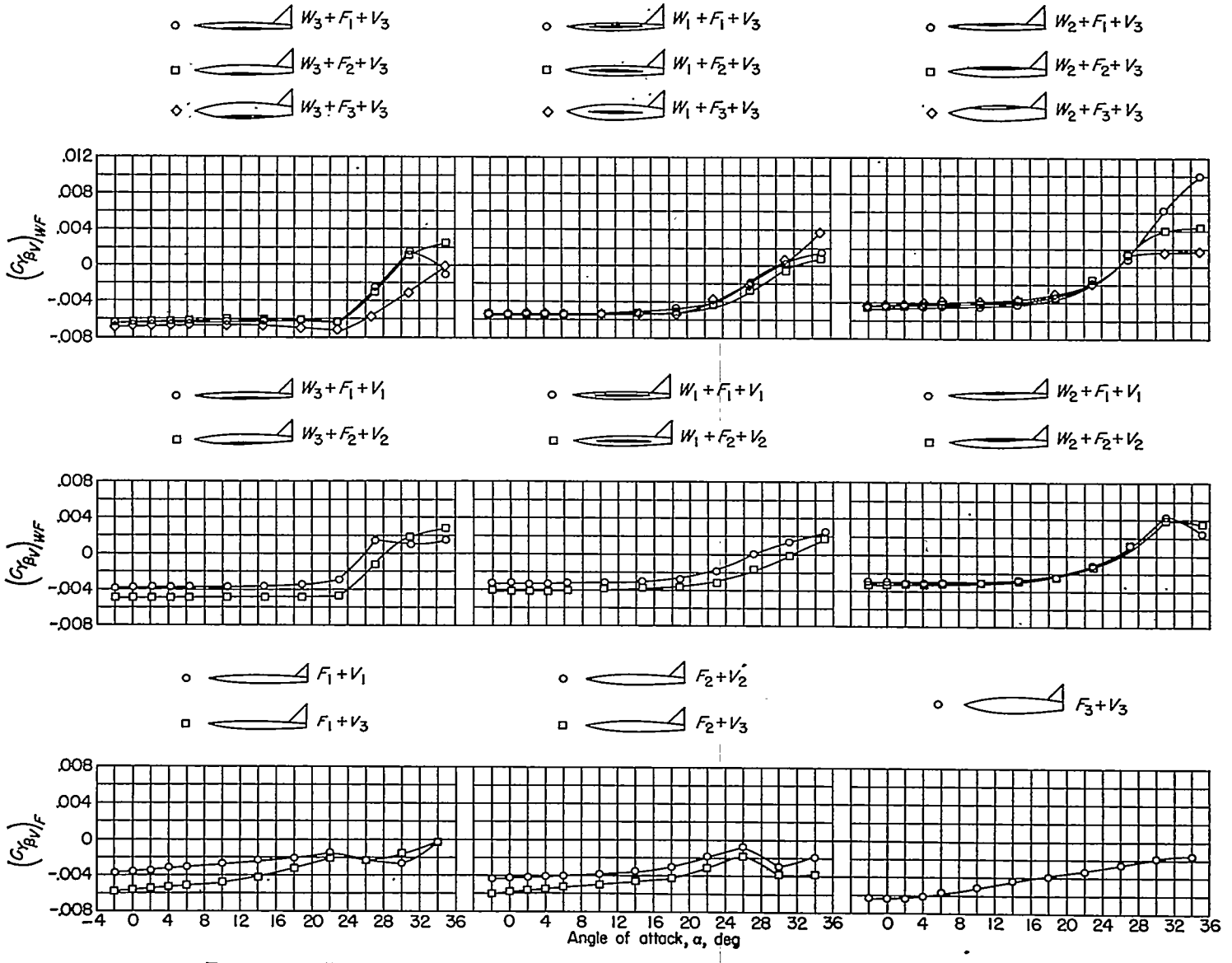

FIGURE 15.—Effects of wing position and fuselage size on the vertical-tail contribution to C_{Y_β}

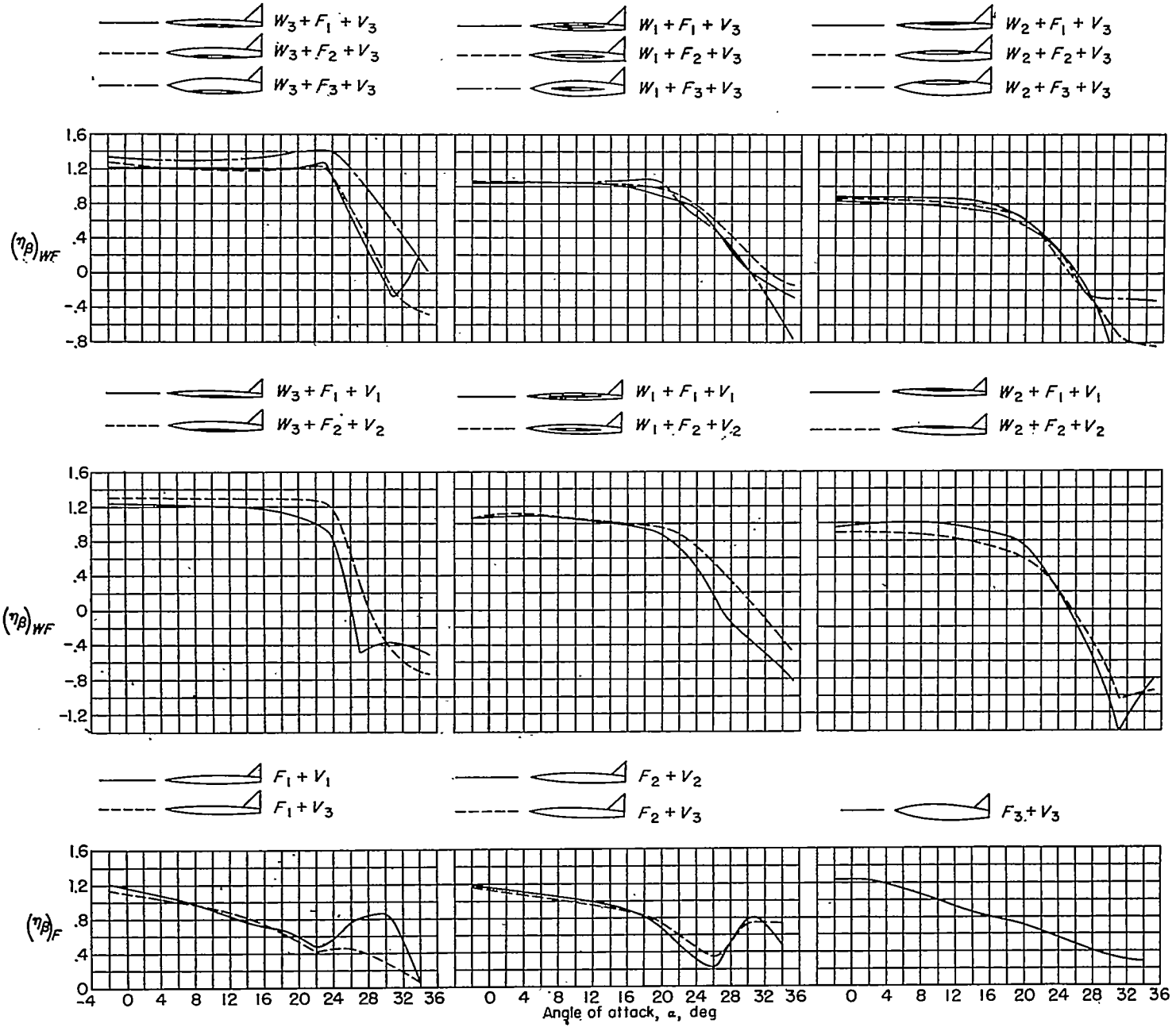

FIGURE 16.—Effects of wing position and fuselage size on the variation of the vertical-tail efficiency factors $(\eta_\beta)_{WF}$ and $(\eta_\beta)_F$ with angle of attack for several wing—fuselage—vertical-tail and fuselage-tail configurations.

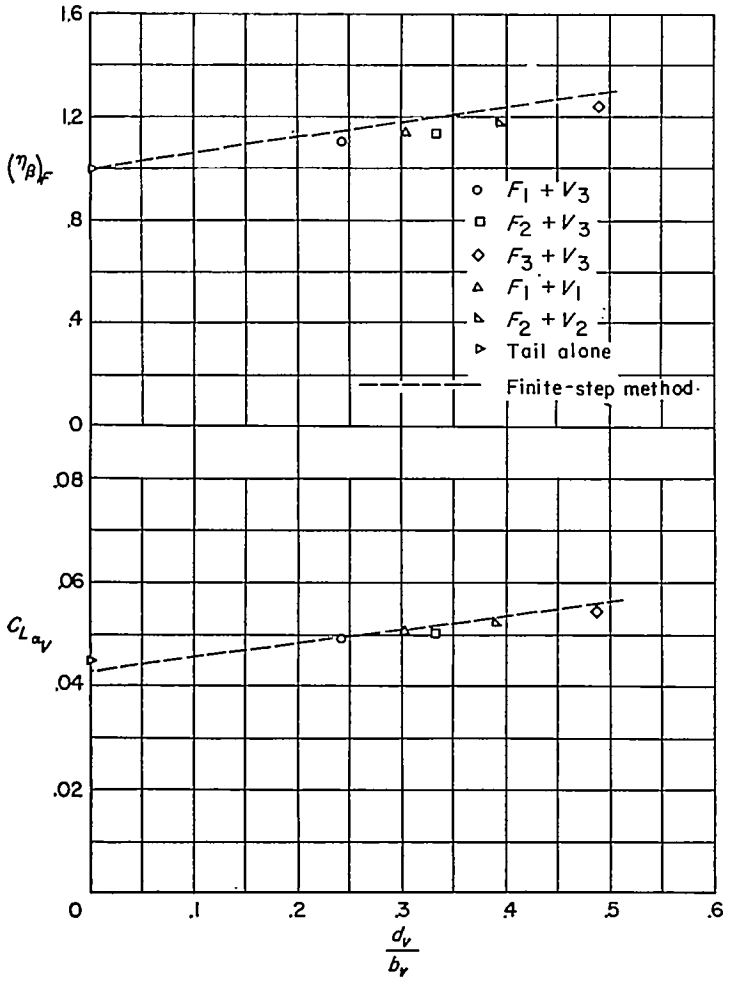

FIGURE 17.—The efficiency factor and vertical-tail lift-curve slope as influenced by the fuselages. $\alpha = 0°$.

Fuselage and fuselage-tail characteristics.—The fuselage and fuselage-tail characteristics are presented in figure 30. The contributions of the fuselages to C_{Y_p} and C_{l_p} are small over the low and moderate angle-of-attack range. The value of C_{n_p} obtained for the fuselages are small and positive and increase slightly with an increase in fuselage size.

The addition of a vertical tail to the fuselages had very little effect on C_{l_p} and made C_{Y_p} slightly more positive at moderate and high angles of attack. Also, the slope for the fuselage-tail configurations $\frac{\partial C_{Y_p}}{\partial \alpha}$ increased with an increase in fuselage size. The vertical-tail contribution made C_{n_p} more positive at low angles of attack, but, at moderate and high angles of attack, C_{n_p} changed sign and became negative. This effect is also indicated by the variation of $(C_{Y_{p_V}})_F$ with angle of attack shown in figure 35.

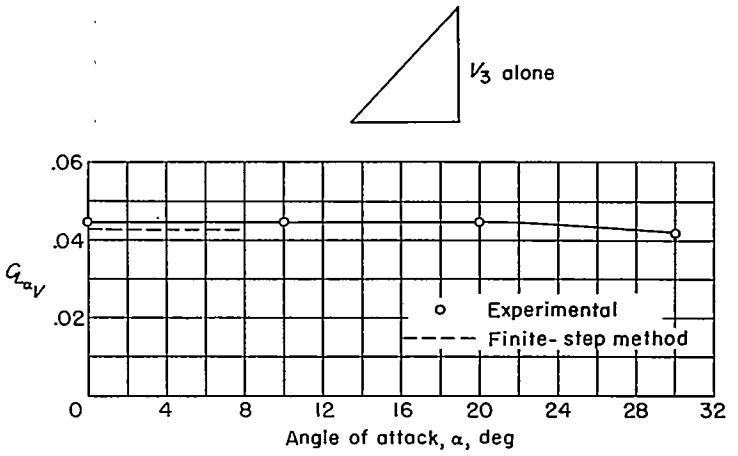

FIGURE 18.—Variation of the isolated-vertical-tail lift-curve slope with angle of attack.

Wing-fuselage characteristics.—The addition of a 60° delta wing in the low, middle, and high positions to the fuselages produced C_{n_p} and C_{l_p} results which are essentially the same as those obtained for the wing alone. (Compare fig. 29 with fig. 31.) In general, at low and moderate angles of attack, the effects of wing position and fuselage size are small for these derivatives. In the case of C_{Y_p}, however, there is a large effect of both wing position and fuselage size. In general, changing the wing position from low to high results in a reduction in the slope $\frac{\partial C_{Y_p}}{\partial \alpha}$. Also, for a given wing position an increase in fuselage size results in an increase in the slope $\frac{\partial C_{Y_p}}{\partial \alpha}$. The wing-fuselage interference increments presented in figure 32 also indicate these trends.

Complete-model characteristics.—The effects of both wing position and fuselage size on the complete-model characteristics are presented in figures 33 and 34. The effects of wing position and fuselage size on the derivative C_{l_p} are generally small, and the variation of this derivative with angle of attack is essentially the same as that obtained for the wing-fuselage configurations (fig. 31). The effects of wing position and fuselage size on the derivative C_{Y_p} are also essentially the same as those obtained for the wing-fuselage configurations in that an increase in fuselage size increases the slope $\frac{\partial C_{Y_p}}{\partial \alpha}$ and a change in wing position from low to high decreases the slope $\frac{\partial C_{Y_p}}{\partial \alpha}$.

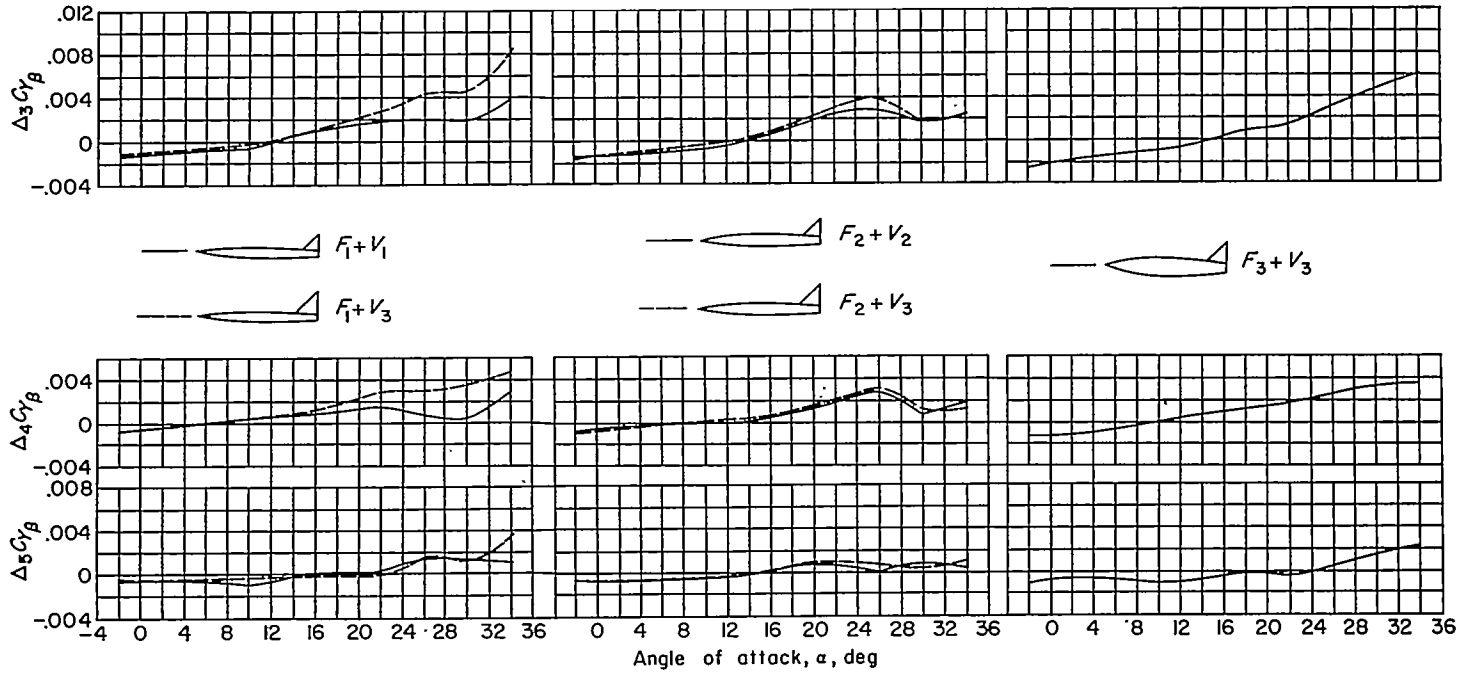

FIGURE 19.—Effects of fuselage size on the fuselage—vertical-tail interference increments $\Delta_3 C_{Y_\beta}$, $\Delta_4 C_{Y_\beta}$, and $\Delta_5 C_{Y_\beta}$.

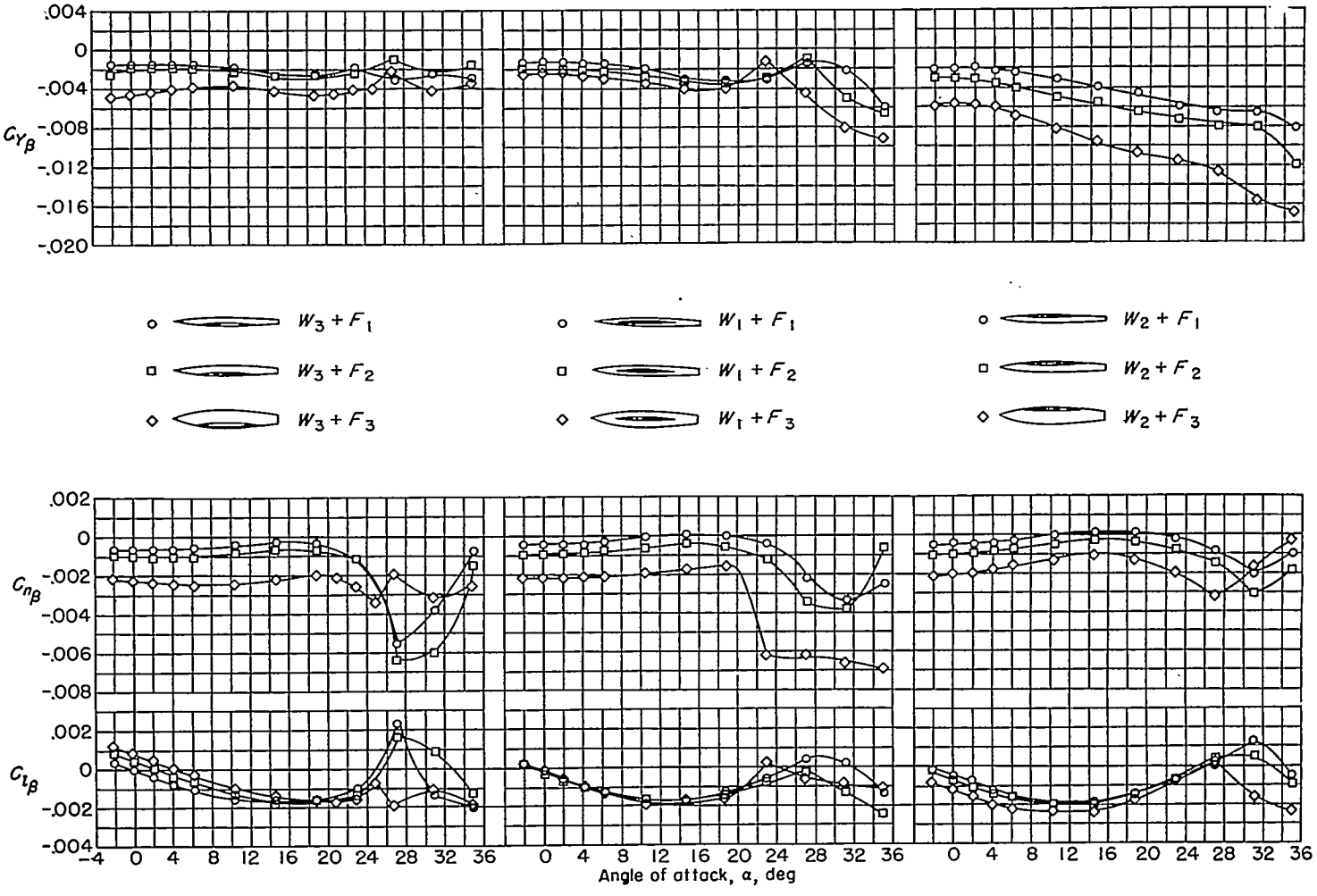

FIGURE 20.—Effects of wing position and fuselage size on the static lateral stability characteristics of several wing-fuselage configurations.

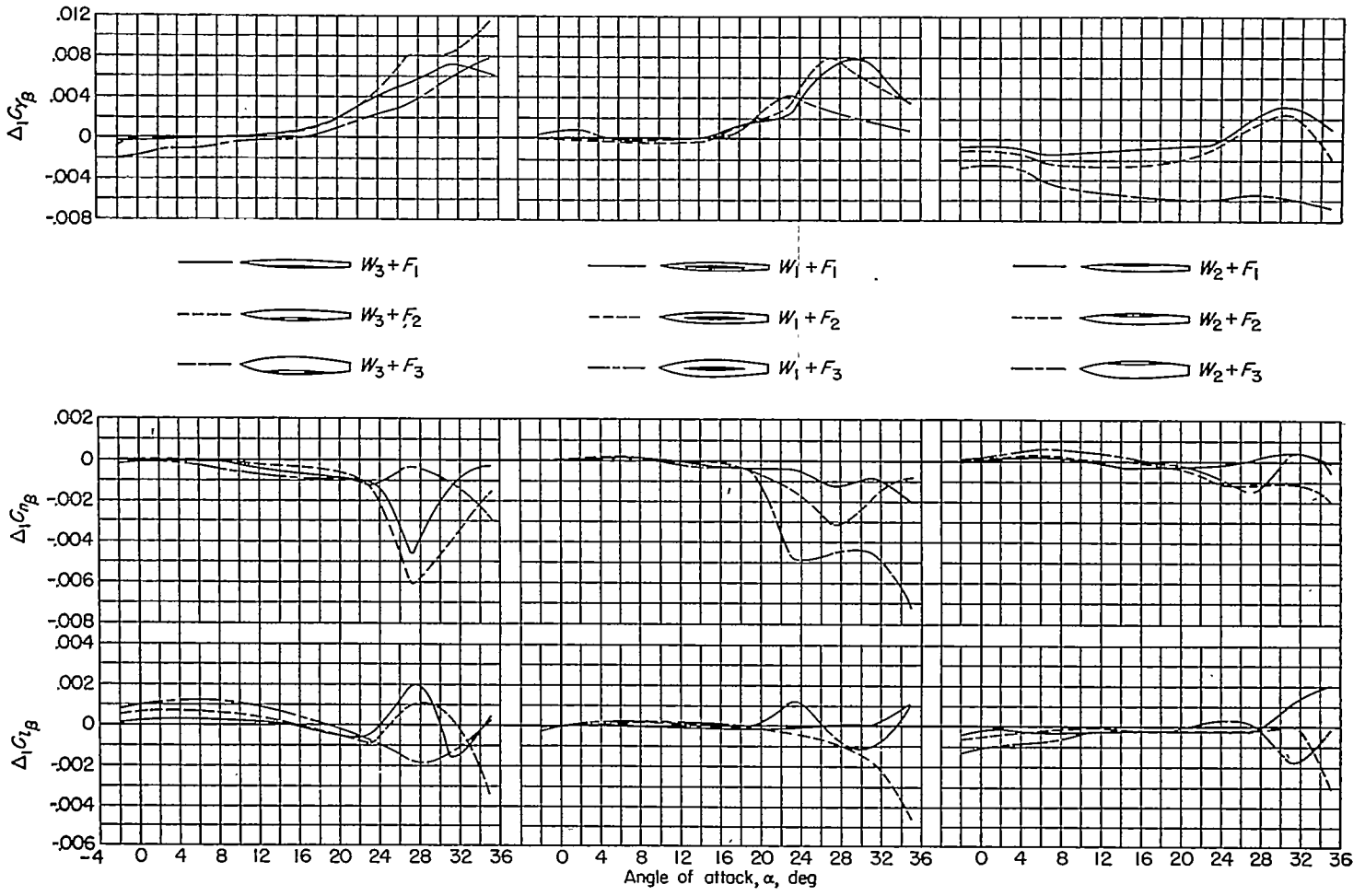

FIGURE 21.—Effects of wing position and fuselage size on the wing-fuselage interference increments $\Delta_1 C_{Y_\beta}$, $\Delta_1 C_{n_\beta}$, and $\Delta_1 C_{l_\beta}$.

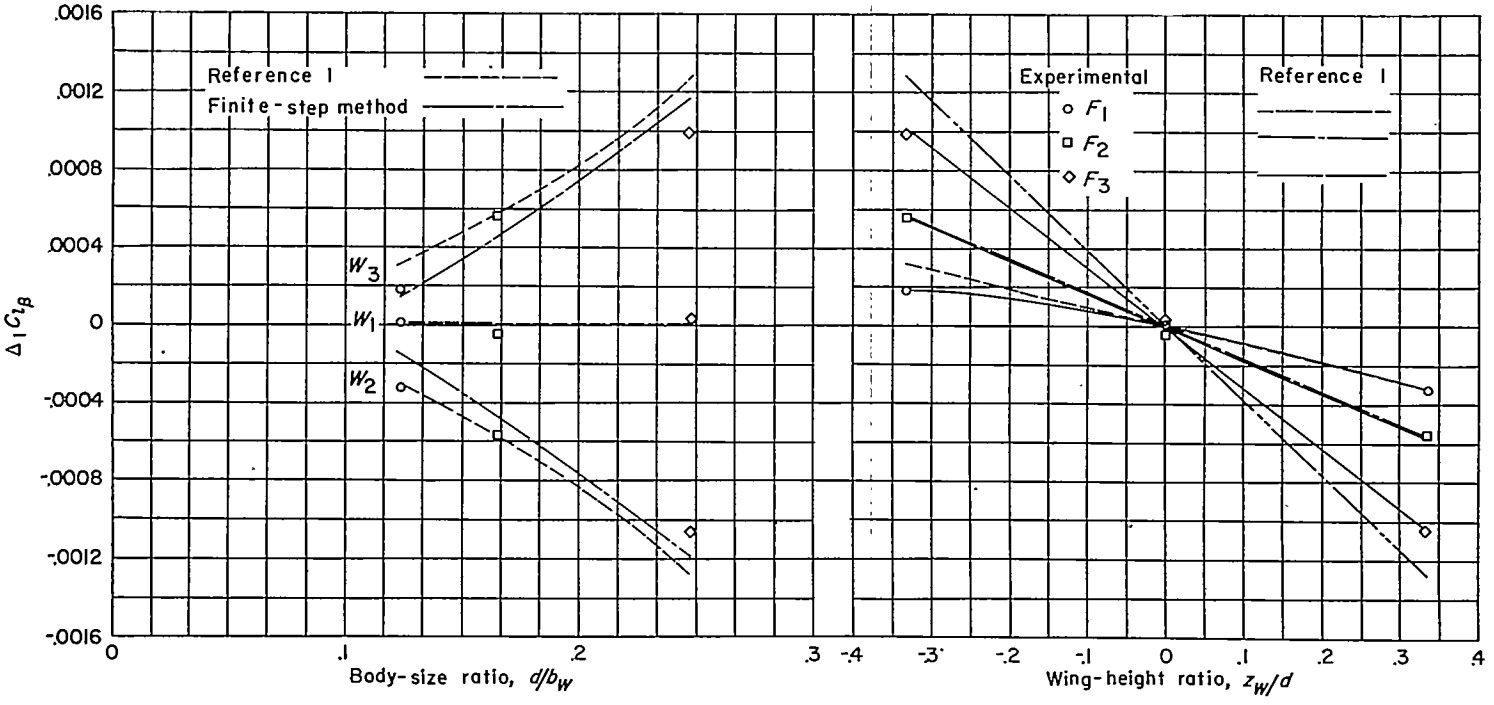

FIGURE 22.—Variation with body-size ratio and wing-height ratio of the wing-fuselage interference increment $\Delta_1 C_{l_\beta}$ for several wing-fuselage configurations. $\alpha=0°$.

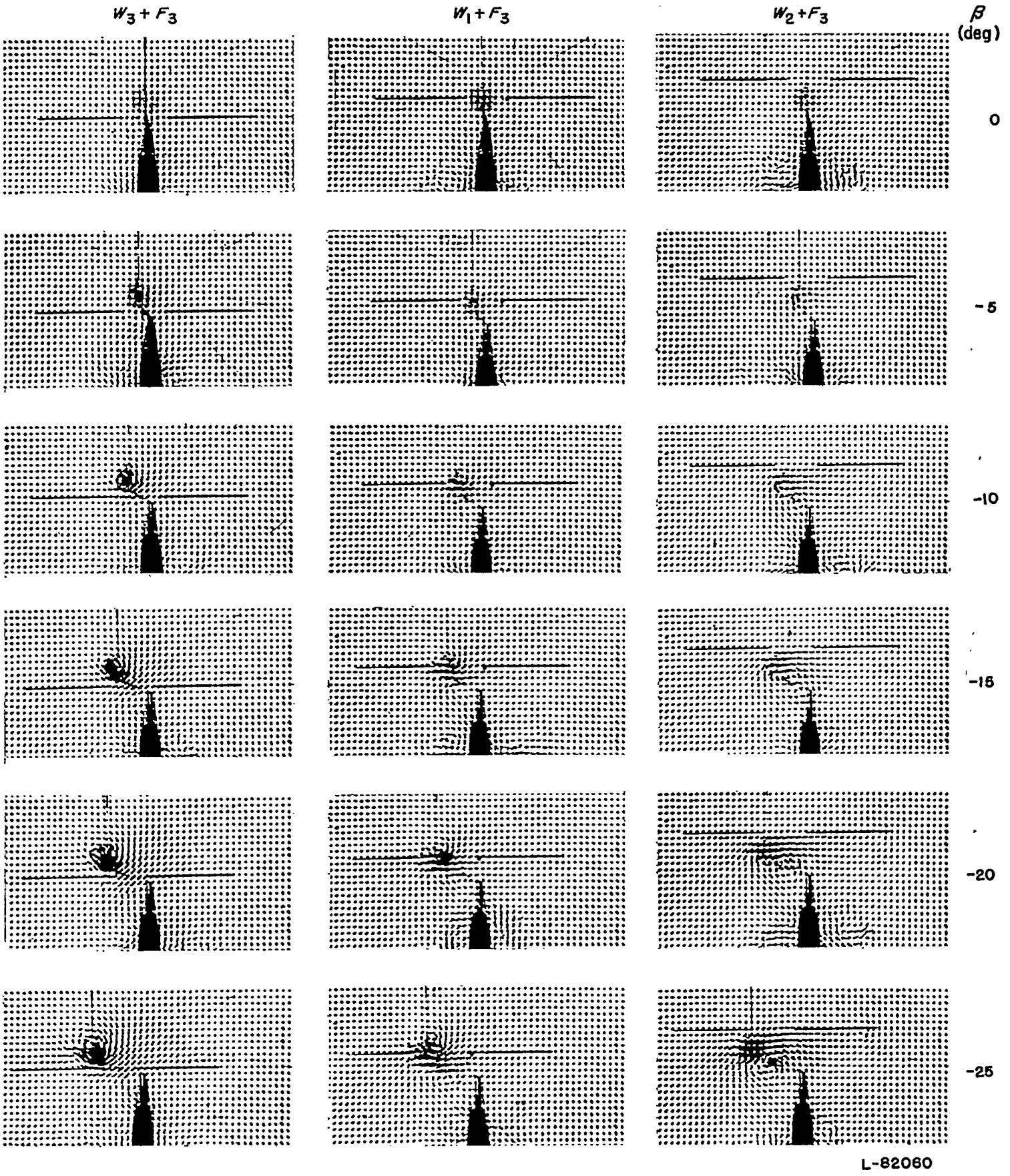

FIGURE 23.—Tuft-grid pictures showing effects of wing position on the sidewash flow at the vertical tail. $\alpha = 0°$.

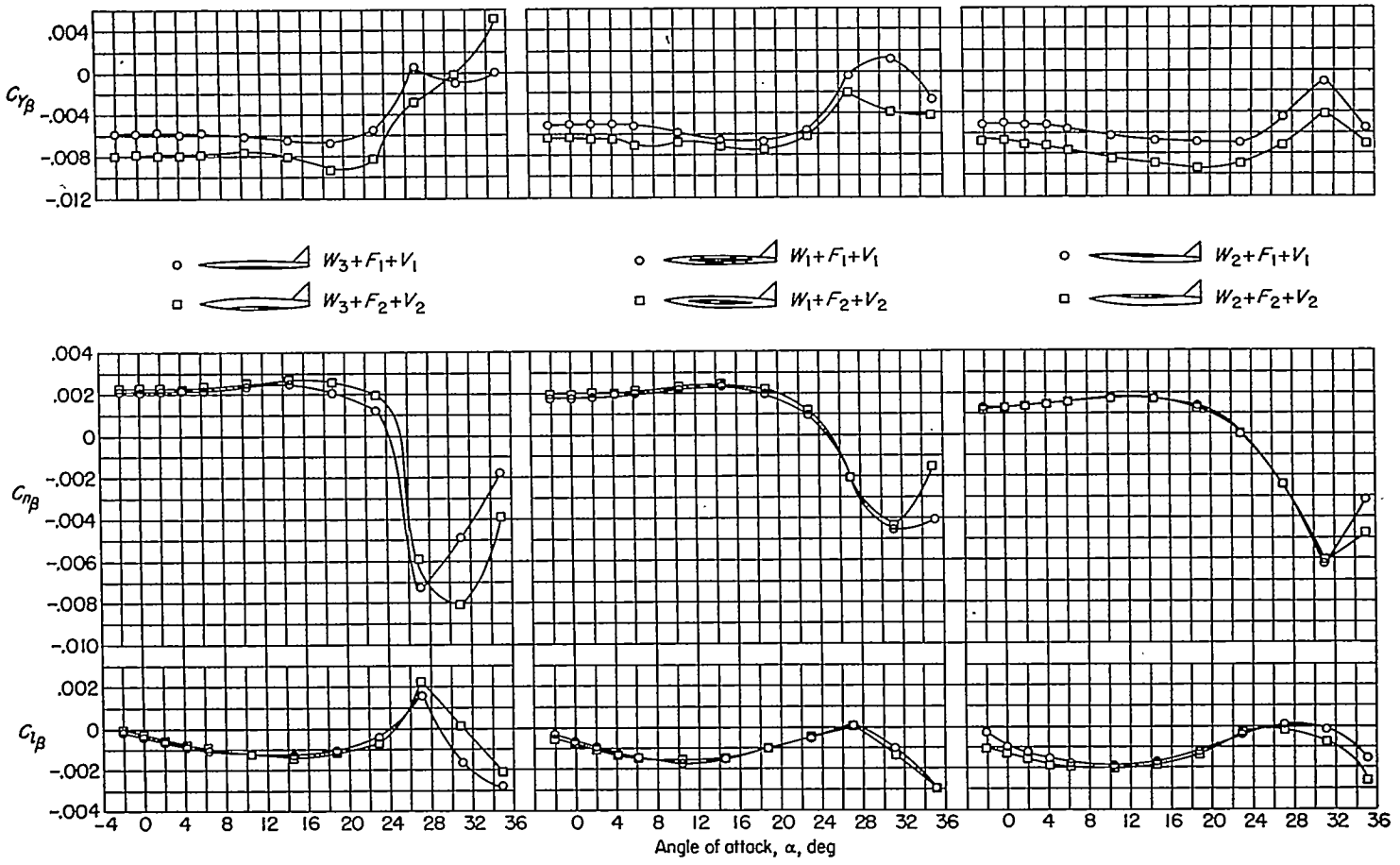

FIGURE 24.—Effects of wing position and fuselage size on the static lateral stability characteristics of several wing—fuselage—vertical-tail configurations. Small and medium vertical tails V_1 and V_2.

Changing the wing position from low to high slightly decreases the negative slope $\frac{\partial C_{n_p}}{\partial \alpha}$ and tends to make C_{n_p} more positive. This effect is also indicated by the variation of the tail contribution $\left(C_{Y_{p_V}}\right)_{WF}$ with angle of attack shown in figure 35. In this case, the slope $\frac{\partial\left(C_{Y_{p_V}}\right)_{WF}}{\partial \alpha}$ decreases when the wing position changes from low to high. These effects are also shown by the interference increments in figures 36 and 37 and by the efficiency factors in figure 38.

The change in the tail contribution $\left(C_{Y_{p_V}}\right)_{WF}$ and in C_{n_p} with a change in wing position can probably be attributed to the shift in the sidewash distribution at the tail with a change in wing position. (See ref. 7.)

CONCLUSIONS

Results of an investigation made to determine the effects of wing position and fuselage size on the low-speed static longitudinal, static lateral, and rolling stability characteristics of airplane models having a triangular wing and vertical tail surfaces indicated the following conclusions:

1. For all wing positions, as the fuselage size was increased the maximum lift coefficient decreased. Also, for a given fuselage size, the maximum lift coefficient increased as the wing position was changed from low to high.

2. The vertical-tail lift-curve slope increased as the fuselage size was increased. This effect could be calculated with good accuracy by using available methods. The results also showed that at low angles of attack the load induced on the vertical tail by the fuselage was equal to the load induced on the fuselage by the vertical tail.

3. As indicated by both available theory and results of previous investigations, the effective dihedral at low angles of attack caused by wing-fuselage interference changed sign as the wing position was changed from low to high. Also, the effective dihedral increased with an increase in fuselage size, that is, from approximately ±2° to ±8°. This effect could be calculated by using available methods.

4. The vertical-tail contribution to the directional stability was increased at low and moderate angles of attack by moving the wing from the high to the low position because of the favorable sidewash at the vertical tail arising from the wing-fuselage interference. At high angles of attack all the configurations investigated became directionally unstable. However, the low-wing—large-fuselage configuration maintained directional stability to an angle of attack above that which corresponds to maximum lift.

5. The effects of wing position and fuselage size on the rolling-stability derivatives were generally small.

LANGLEY AERONAUTICAL LABORATORY,
NATIONAL ADVISORY COMMITTEE FOR AERONAUTICS,
LANGLEY FIELD, VA., *November 4, 1953.*

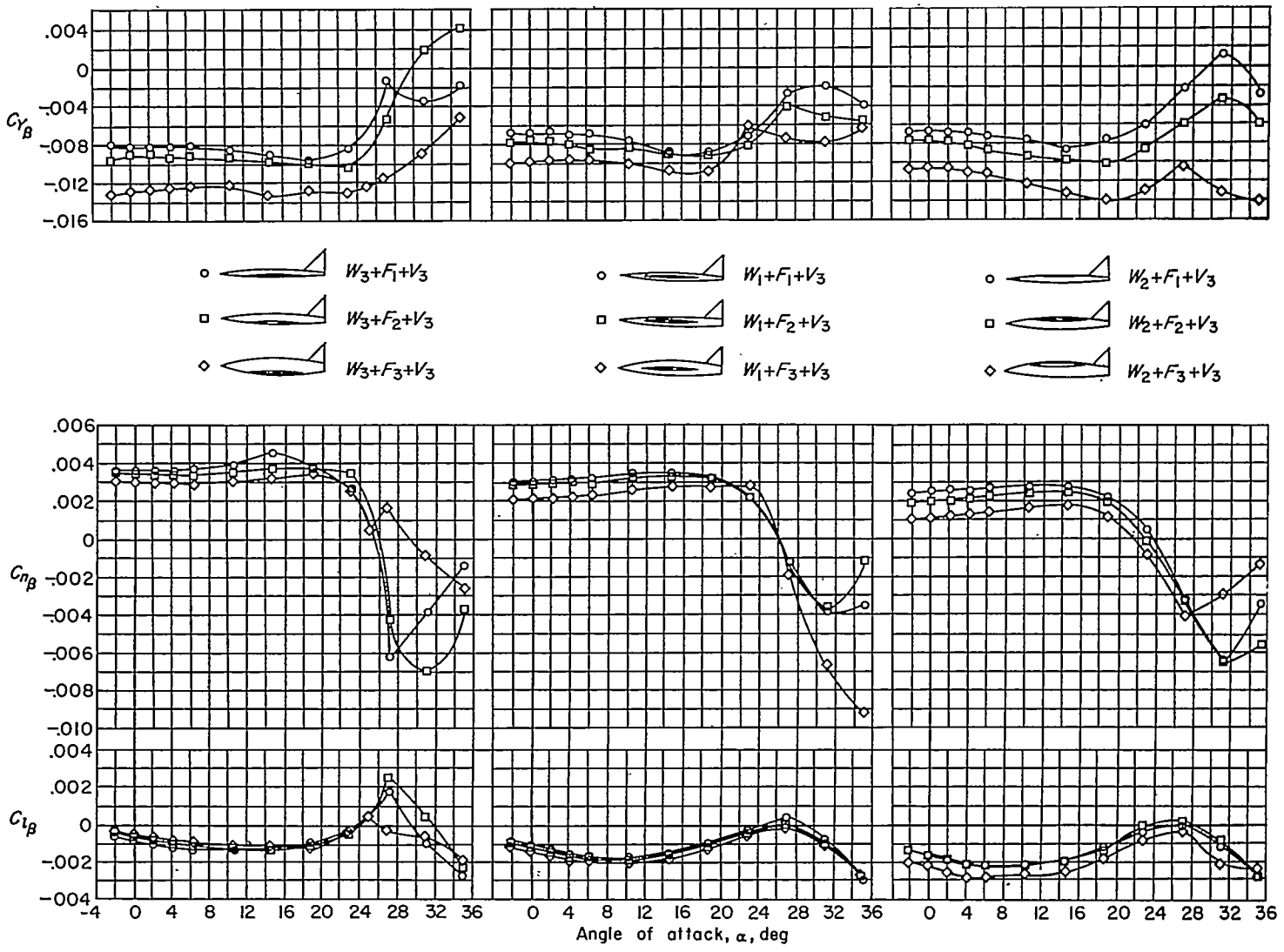

FIGURE 25.—Effects of wing position and fuselage size on the static lateral stability characteristics of several wing—fuselage—vertical-tail configurations. Large vertical tail V_3.

REFERENCES

1. Campbell, John P., and McKinney, Marion O.: Summary of Methods for Calculating Dynamic Lateral Stability and Response and for Estimating Lateral Stability Derivatives. NACA Rep. 1098, 1952. (Supersedes NACA TN 2409.)
2. Goodman, Alex: Effects of Wing Position and Horizontal-Tail Position on the Static Stability Characteristics of Models With Unswept and 45° Sweptback Surfaces With Some Reference to Mutual Interference. NACA TN 2504, 1951.
3. MacLachlan, Robert, and Letko, William: Correlation of Two Experimental Methods of Determining the Rolling Characteristics of Unswept Wings. NACA TN 1309, 1947.
4. Bird, John D., and Riley, Donald R.: Some Experiments on Visualization of Flow Fields Behind Low-Aspect-Ratio Wings by Means of a Tuft Grid. NACA TN 2674, 1952.
5. Silverstein, Abe, and White, James A.: Wind-Tunnel Interference With Particular Reference to Off-Center Positions of the Wing and to the Downwash at the Tail. NACA Rep. 547, 1936.
6. House, Rufus O., and Wallace, Arthur R.: Wind-Tunnel Investigation of Effect of Interference on Lateral-Stability Characteristics of Four NACA 23012 Wings, an Elliptical and a Circular Fuselage, and Vertical Fins. NACA Rep. 705, 1941.
7. Michael, William H., Jr.: Analysis of the Effects of Wing Interference on the Tail Contributions to the Rolling Derivatives. NACA Rep. 1086, 1952. (Supersedes NACA TN 2332.)
8. DeYoung, John: Theoretical Additional Span Loading Characteristics of Wings With Arbitrary Sweep, Aspect Ratio, and Taper Ratio. NACA TN 1491, 1947.
9. Munk, Max M.: The Aerodynamic Forces on Airship Hulls. NACA Rep. 184, 1924.
10. Lichtenstein, Jacob H.: Experimental Determination of the Effect of Horizontal-Tail Size, Tail Length, and Vertical Location on Low-Speed Static Longitudinal Stability and Damping in Pitch of a Model Having 45° Sweptback Wing and Tail Surfaces. NACA Rep. 1096, 1952. (Supersedes NACA TN's 2381 and 2382.)
11. Ribner, Herbert S.: The Stability Derivatives of Low-Aspect-Ratio Triangular Wings at Subsonic and Supersonic Speeds. NACA TN 1423, 1947.
12. Queijo, M. J., and Wolhart, Walter D.: Experimental Investigation of the Effect of Vertical-Tail Size and Length and of Fuselage Shape and Length on the Static Lateral Stability Characteristics of a Model With 45° Sweptback Wing and Tail Surfaces. NACA Rep. 1049, 1951. (Supersedes NACA TN 2168.)

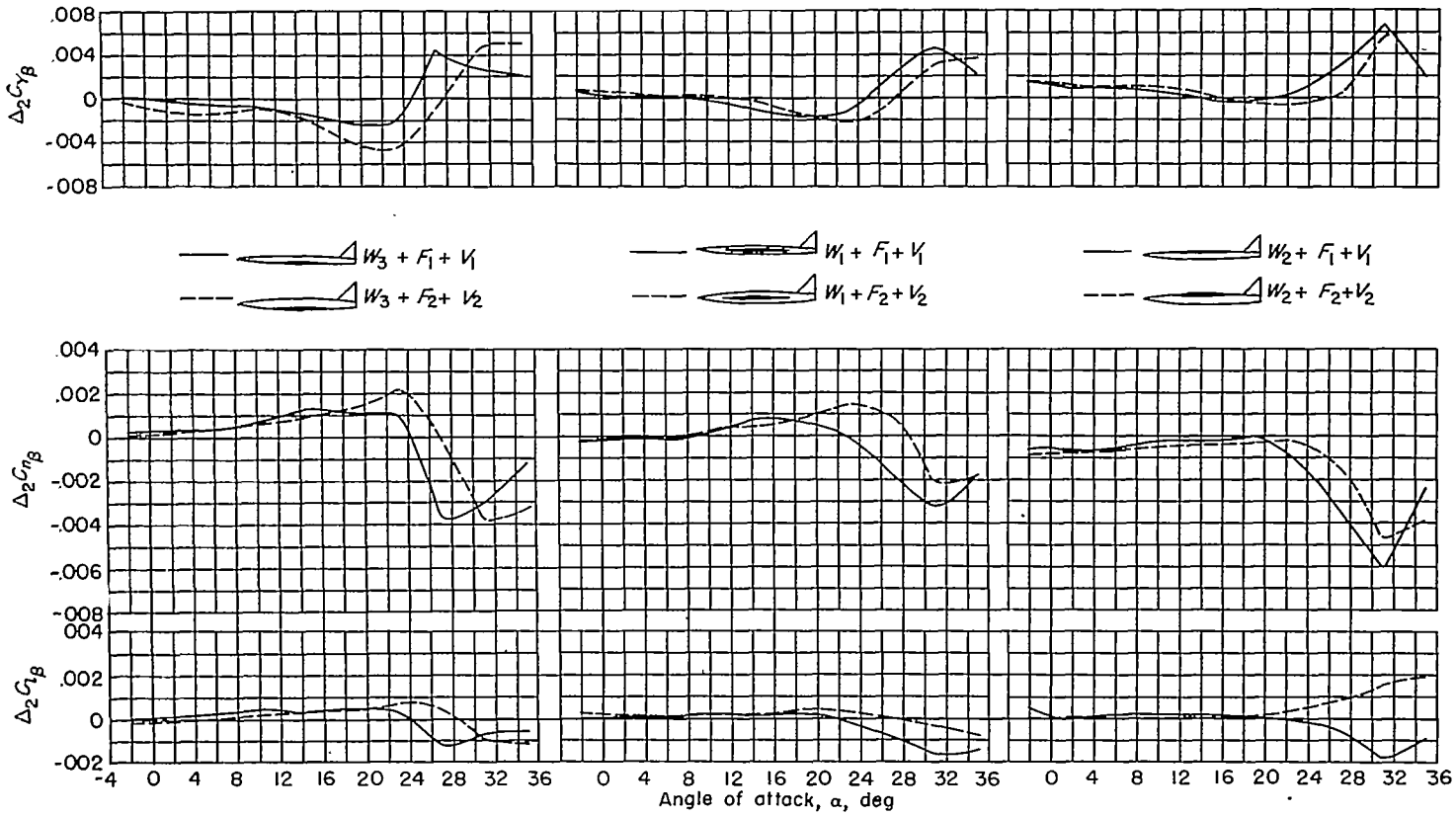

FIGURE 26.—Effects of wing position and fuselage size on the increments caused by wing-fuselage interference on the vertical-tail contributions $\Delta_2 C_{Y_\beta}$, $\Delta_2 C_{n_\beta}$, and $\Delta_2 C_{l_\beta}$. Small and medium vertical tails V_1 and V_2.

13. Spreiter, John R.: The Aerodynamic Forces on Slender Plane- and Cruciform-Wing and Body Combinations. NACA Rep. 962, 1950. (Supersedes NACA TN's 1897 and 1662.)

14. Riley, Donald R.: Effect of Horizontal-Tail Span and Vertical Location on the Aerodynamic Characteristics of an Unswept Tail Assembly in Sideslip. NACA Rep. 1171, 1954. (Supersedes NACA TN 2907.)

15. Zlotnick, Martin, and Robinson, Samuel W., Jr.: A Simplified Mathematical Model for Calculating Aerodynamic Loading and Downwash for Wing-Fuselage Combinations With Wings of Arbitrary Plan Form. NACA TN 3057, 1954. (Supersedes NACA RM L52J27a.)

16. Michael, William H., Jr.: Investigation of Mutual Interference Effects of Several Vertical-Tail—Fuselage Configurations in Sideslip. NACA TN 3135, 1954.

17. Schlichting, H.: Aerodynamics of the Mutual Influence of Aircraft Parts (Interference). Library Translation No. 275, British R.A.E., Oct. 1948.

18. Glauert, H.: The Elements of Aerofoil and Airscrew Theory. Second ed., Cambridge Univ. Press, 1947. (Reprinted 1948.)

19. Jacobs, W.: Lift and Moment Changes Due to the Fuselage for a Yawed Aeroplane With Unswept and Swept Wings. Rep. No. 34, Aero. Res. Inst. of Sweden (Stockholm), 1950.

20. Goodman, Alex, and Adair, Glenn H.: Estimation of the Damping in Roll of Wings Through the Normal Flight Range of Lift Coefficient. NACA TN 1924, 1949.

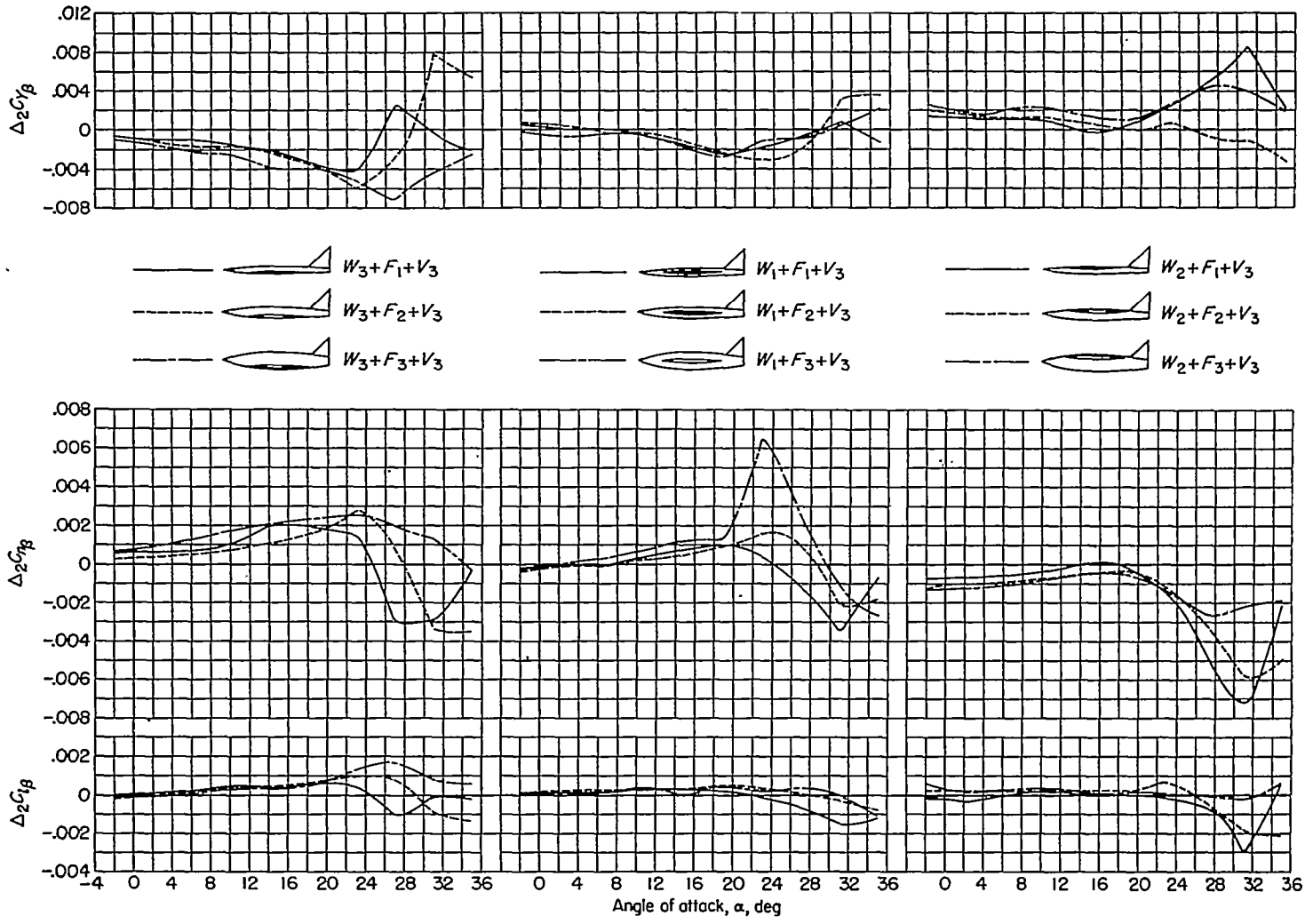

FIGURE 27.—Effects of wing position and fuselage size on the increments caused by wing-fuselage interference on the vertical-tail contribution $\Delta_2 C_{Y_\beta}$, $\Delta_2 C_{n_\beta}$, and $\Delta_2 C_{l_\beta}$. Large vertical tail V_3.

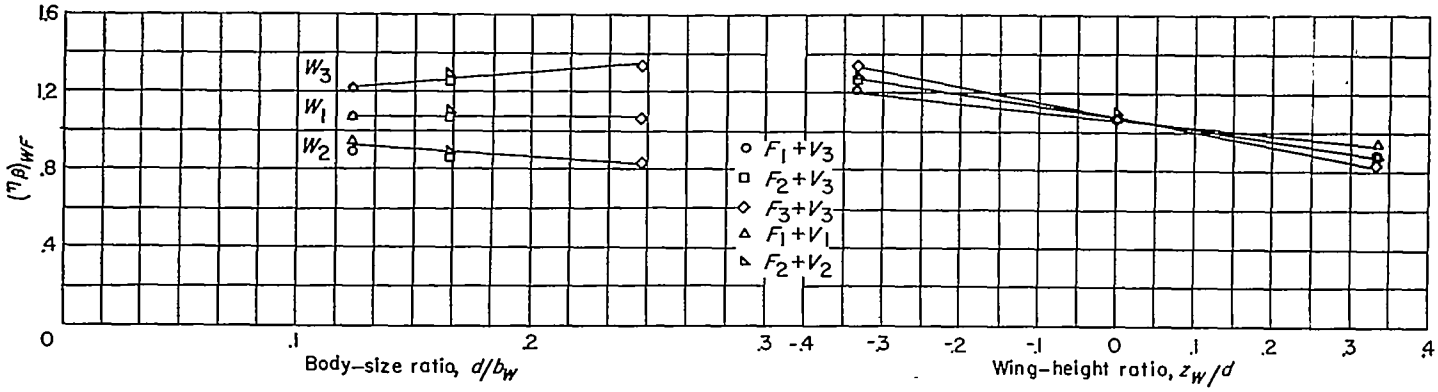

FIGURE 28.—Variations of the vertical-tail efficiency factor $(\eta_\beta)_{WF}$ with body-size ratio and wing-height ratio. $\alpha=0°$.

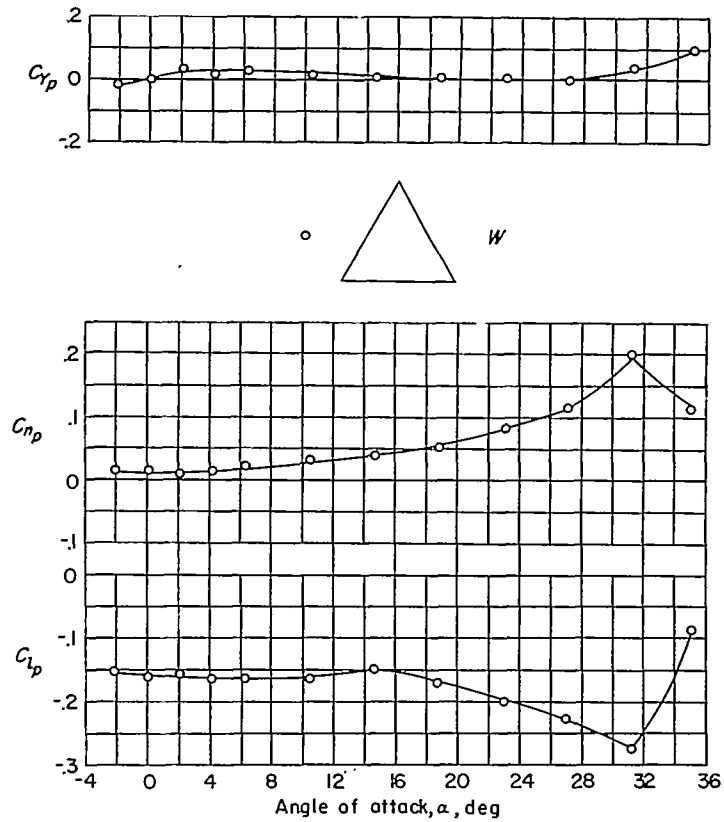

FIGURE 29.—Rolling stability characteristics of the 60° delta wing.

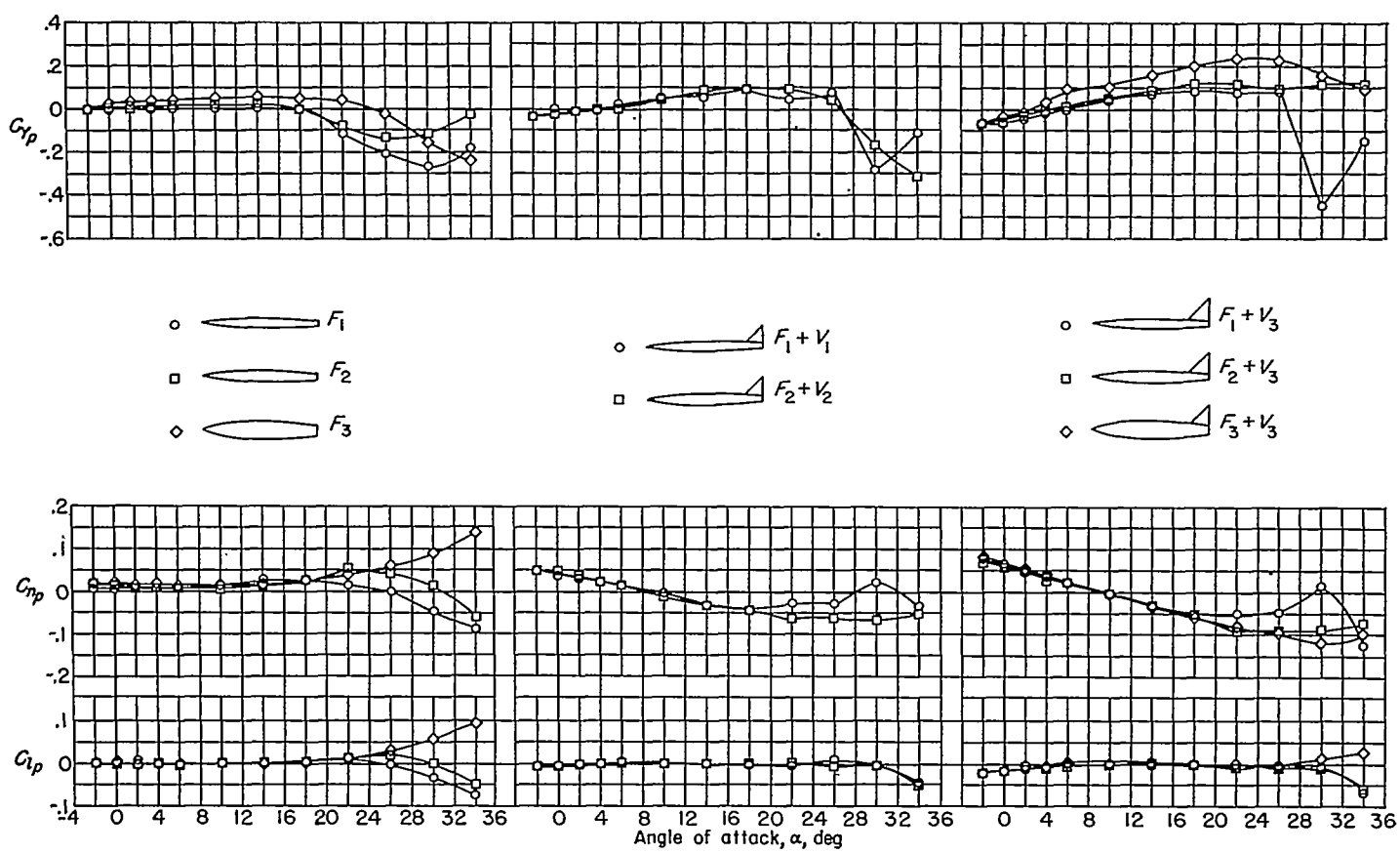

FIGURE 30.—Rolling stability characteristics of the fuselages and the fuselages in combination with several vertical tails.

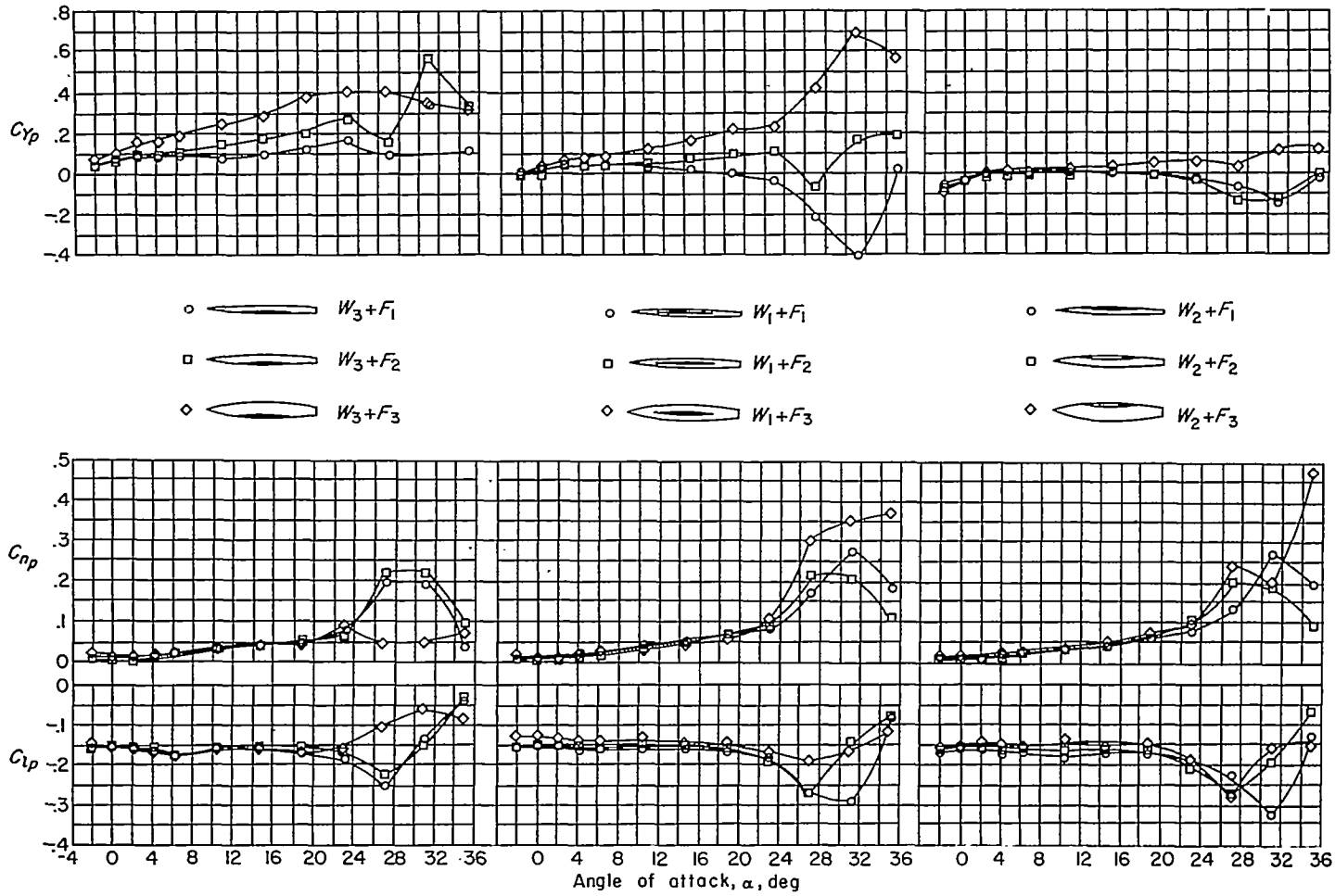

FIGURE 31.—Effects of wing position and fuselage size on the rolling stability characteristics of several wing-fuselage combinations.

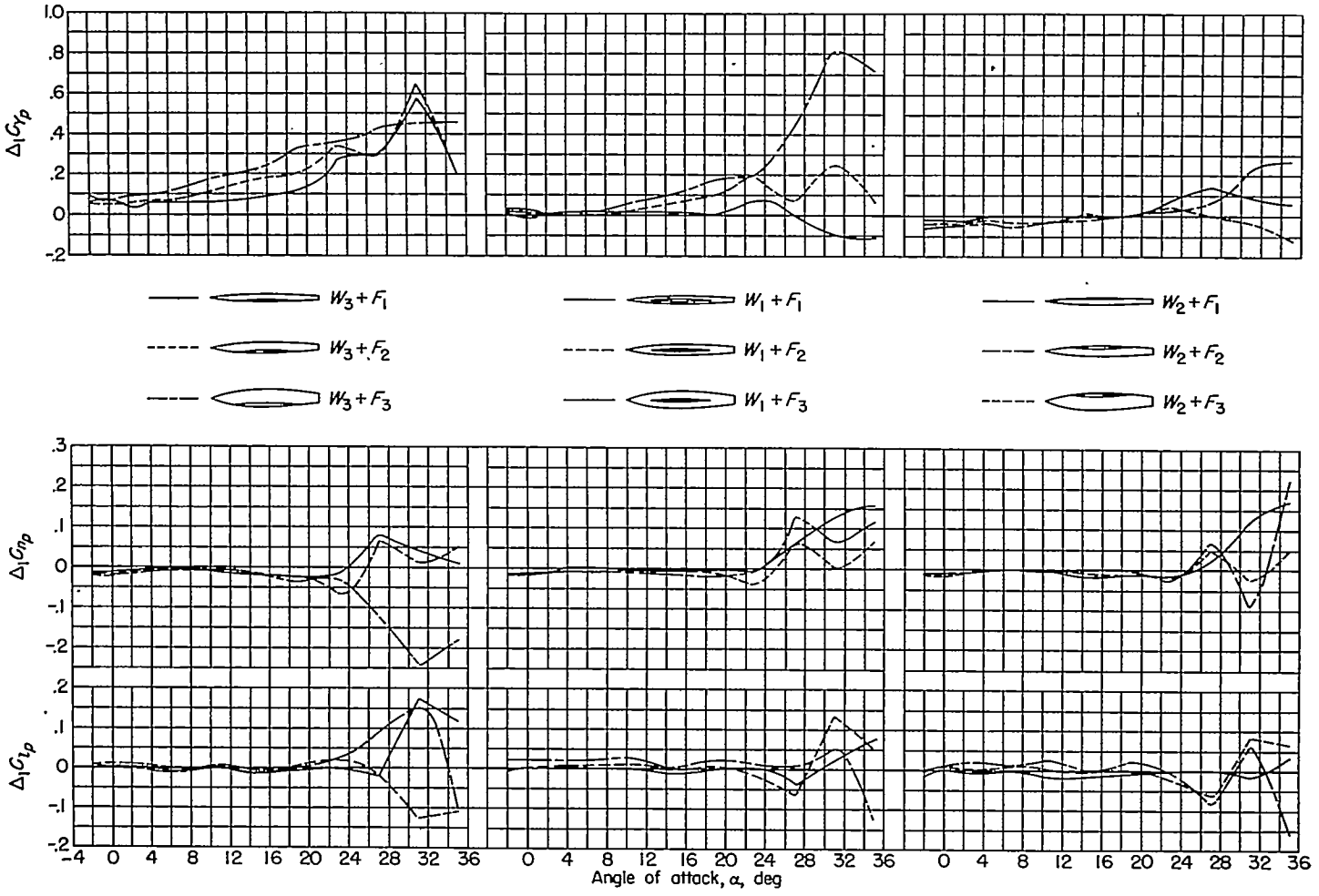

FIGURE 32.—Effects of wing position and fuselage size on the wing-fuselage interference increments $\Delta_1 C_{Y_p}$, $\Delta_1 C_{n_p}$, and $\Delta_1 C_{l_p}$.

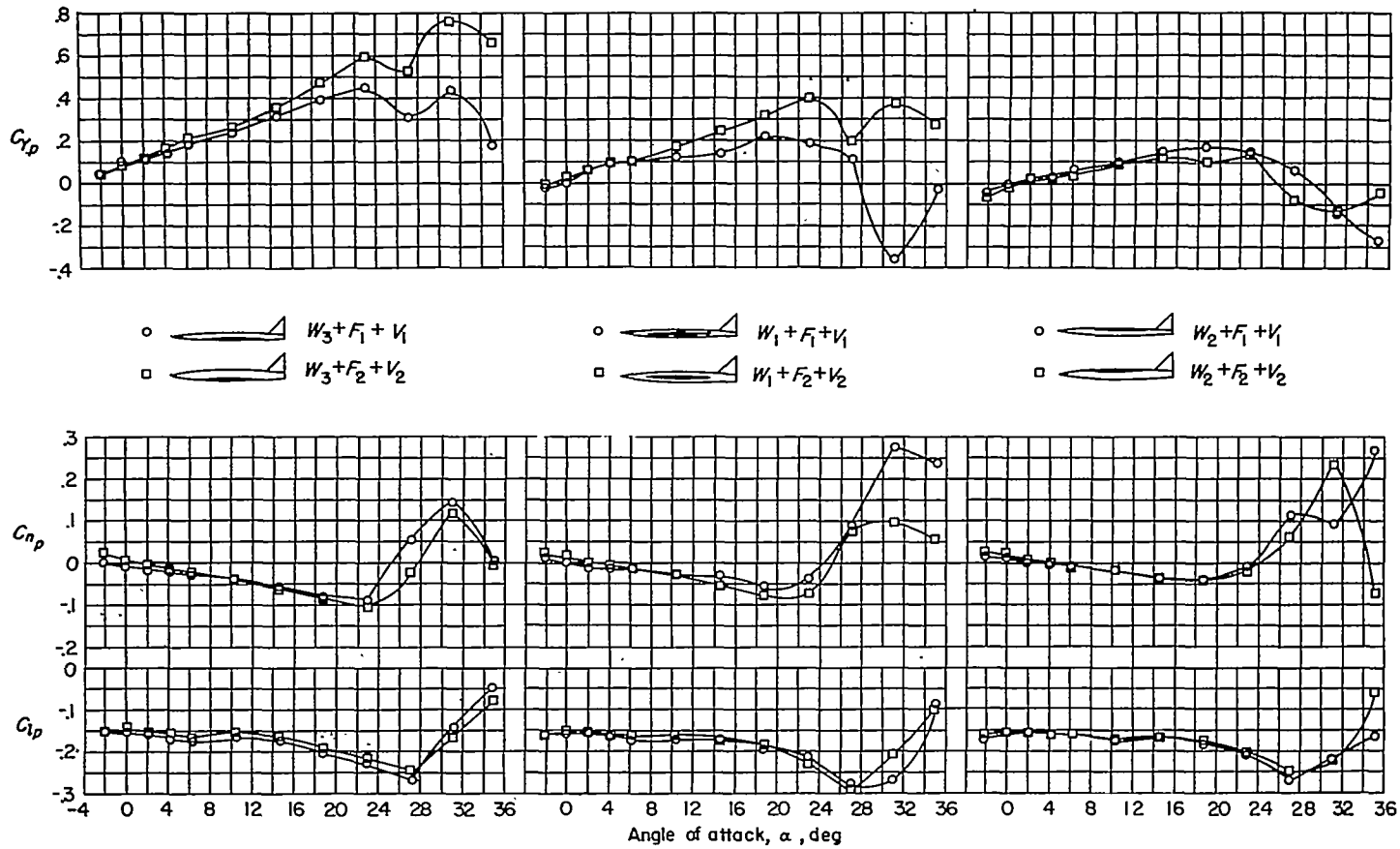

FIGURE 33.—Effects of wing position and fuselage size on the rolling stability characteristics of several wing—fuselage—vertical-tail configurations. Small and medium vertical tails V_1 and V_2.

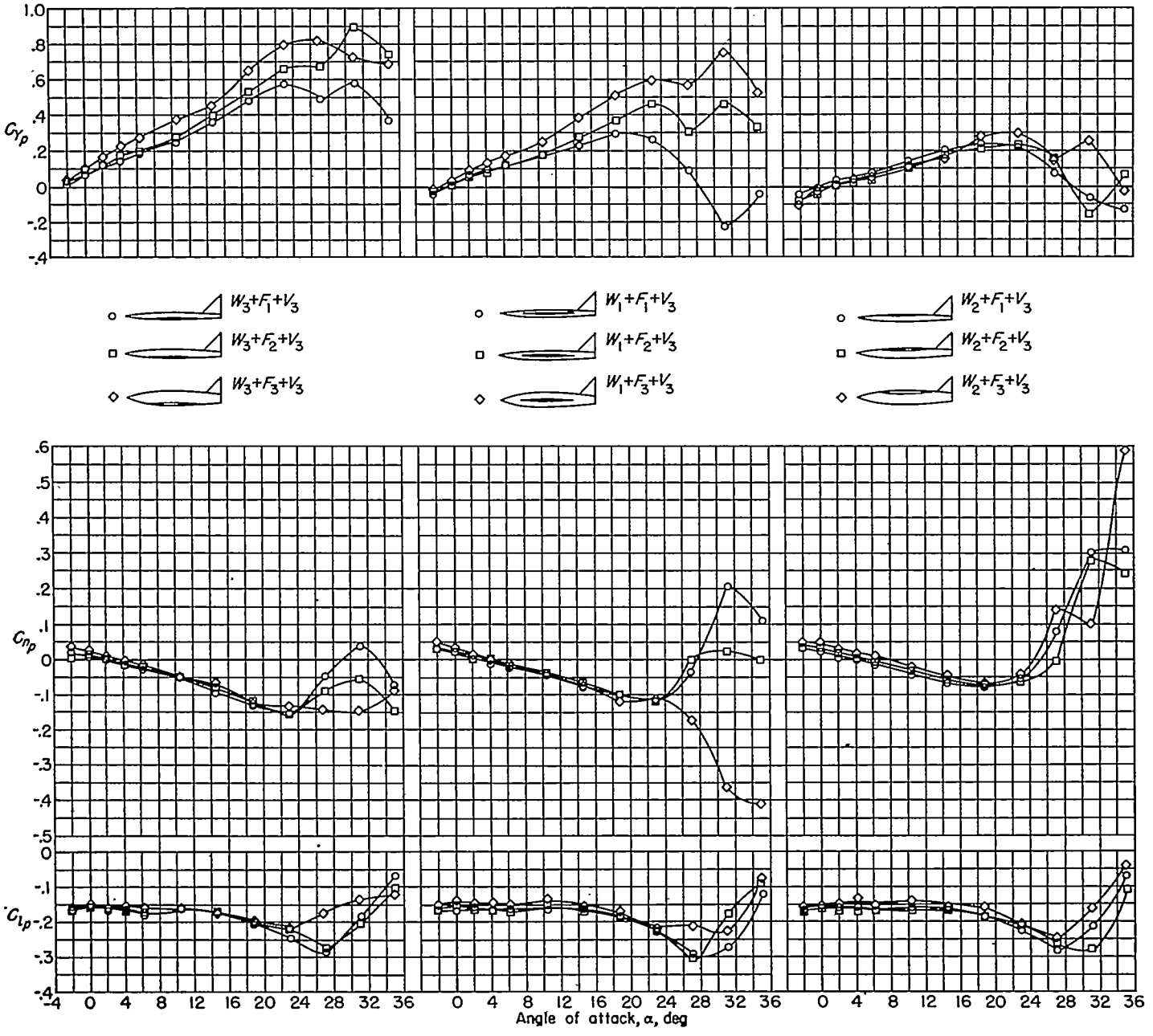

FIGURE 34.—Effects of wing position and fuselage size on the rolling stability characteristics of several wing—fuselage—vertical-tail configurations. Large vertical tail V_3.

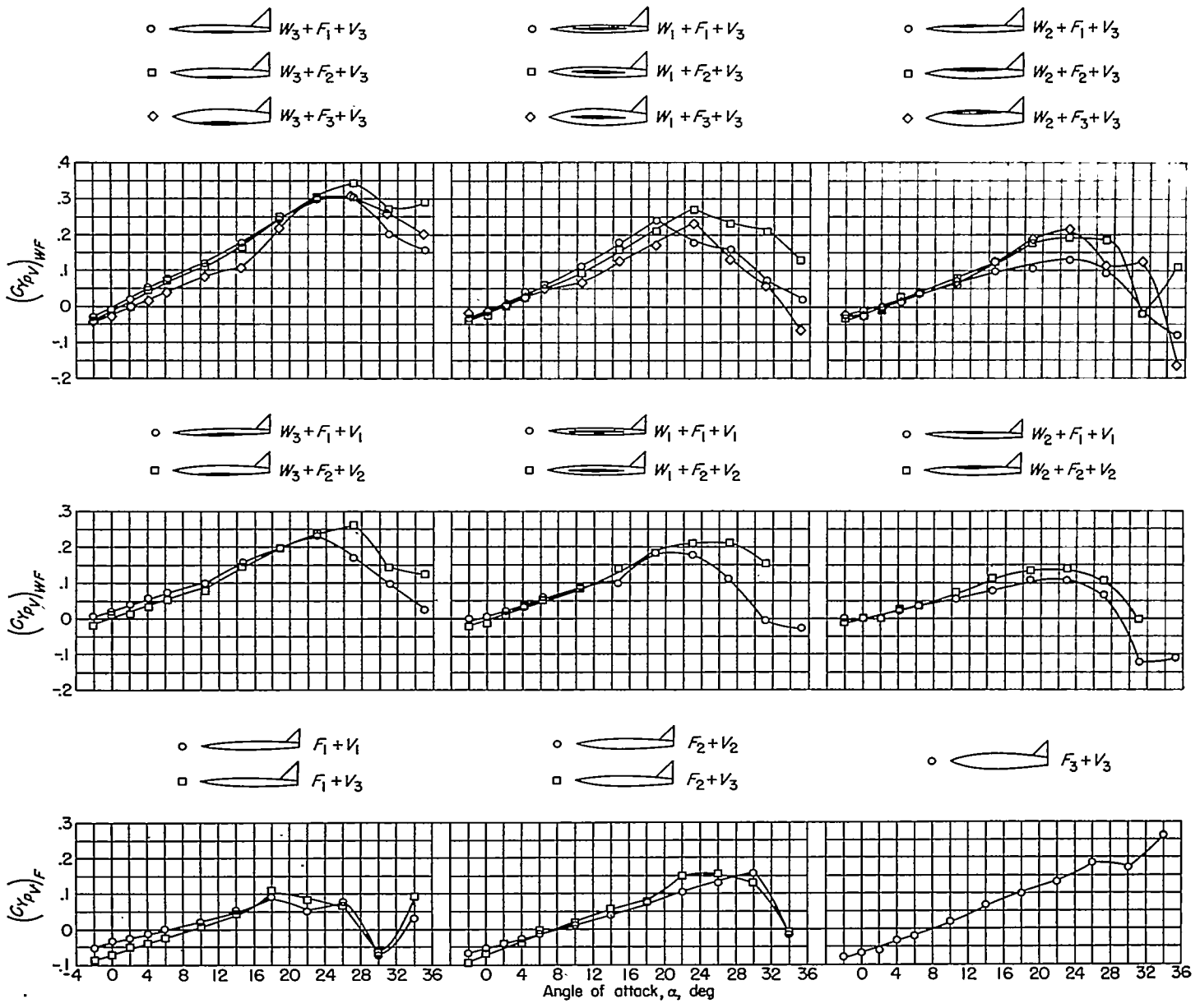

FIGURE 35.—Effects of wing position and fuselage size on the vertical tail contribution to C_{Y_p}.

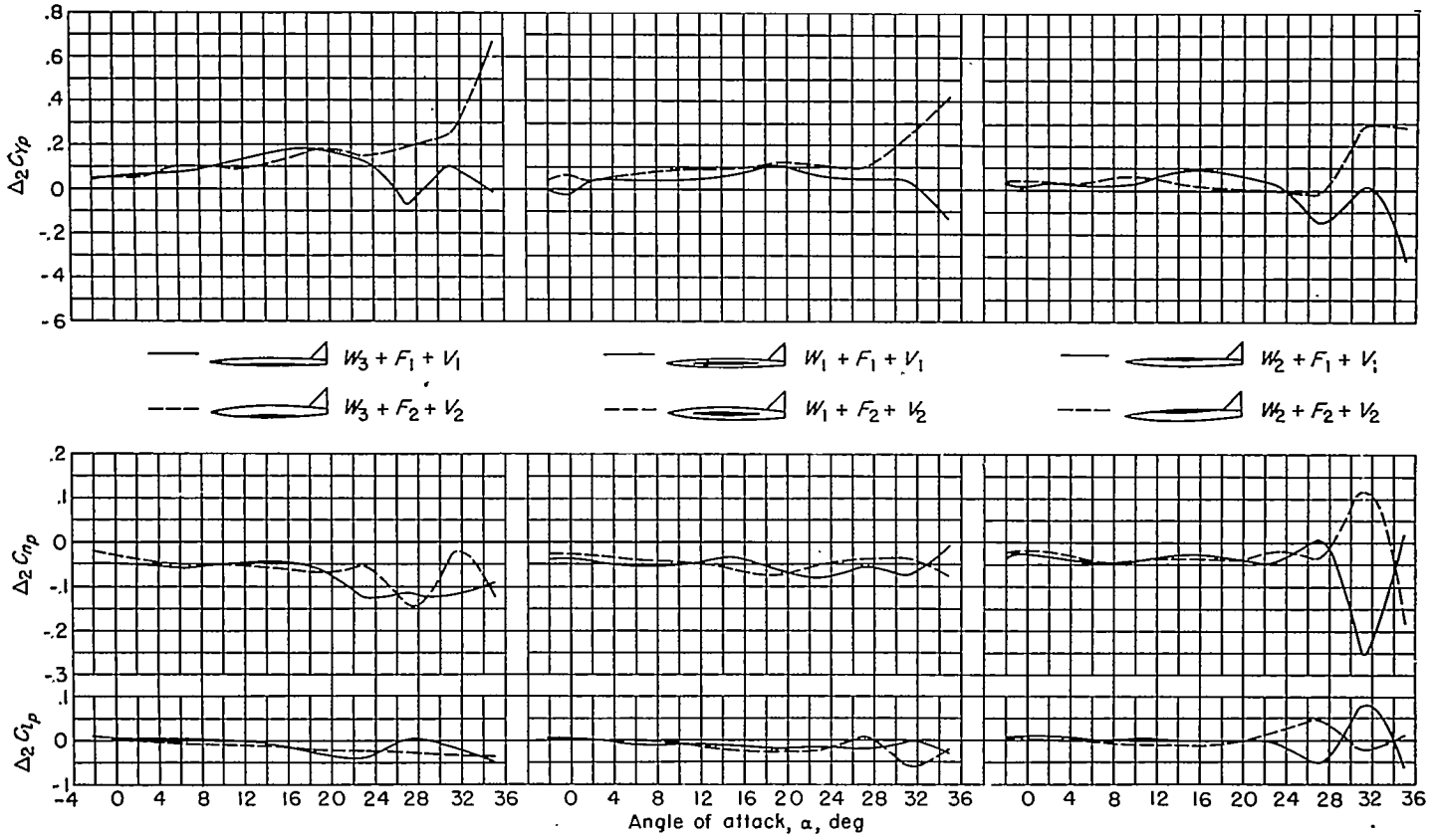

FIGURE 36.—Effects of wing position and fuselage size on the increments caused by wing-fuselage interference on the vertical-tail contributions $\Delta_2 C_{Y_p}$, $\Delta_2 C_{n_p}$, and $\Delta_2 C_{l_p}$. Small and medium vertical tails V_1 and V_2.

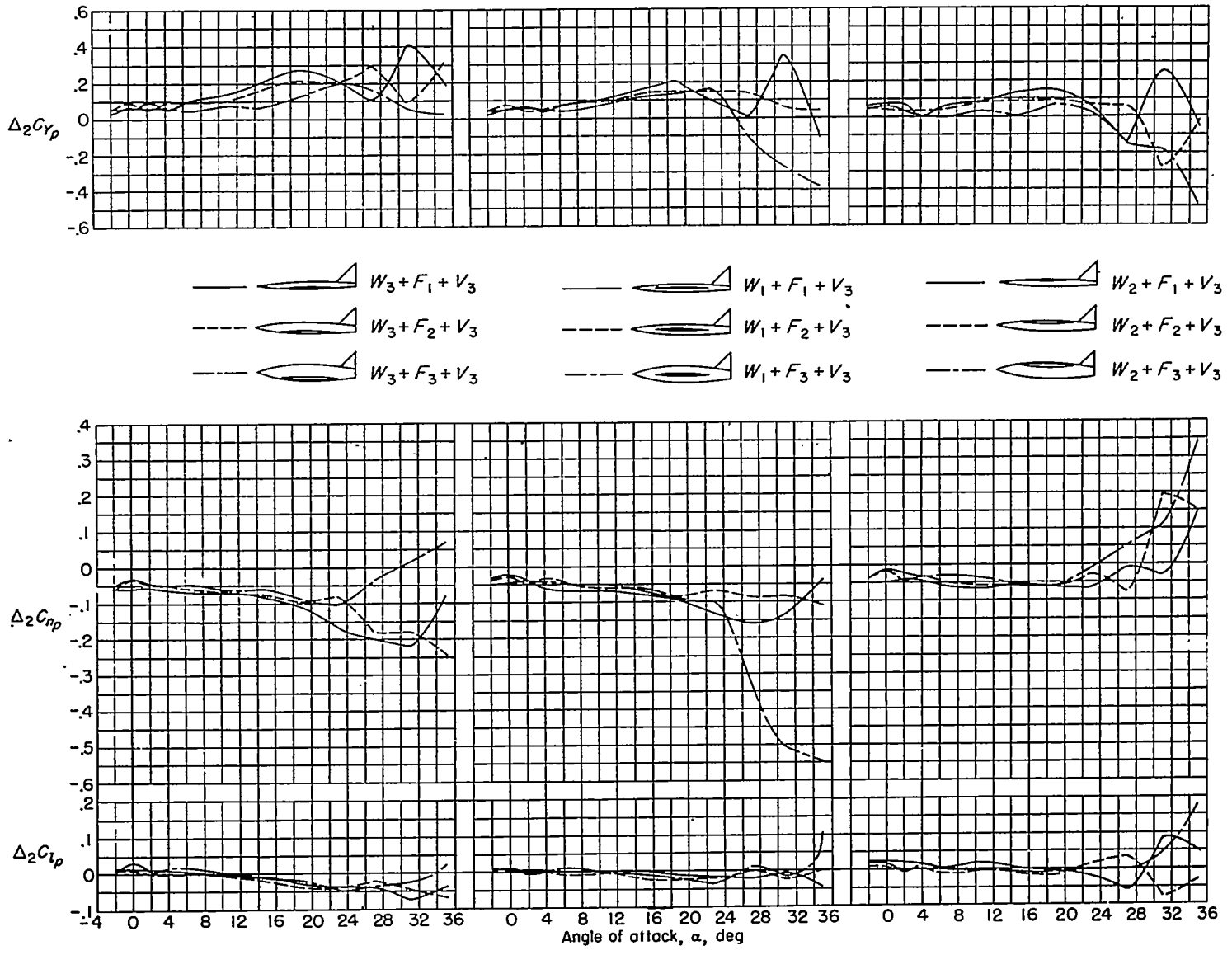

FIGURE 37.—Effects of wing position and fuselage size on the increments caused by wing-fuselage interference on the vertical-tail contributions $\Delta_2 C_{Y_p}$, $\Delta_2 C_{n_p}$, and $\Delta_2 C_{l_p}$. Large vertical tail V_3.

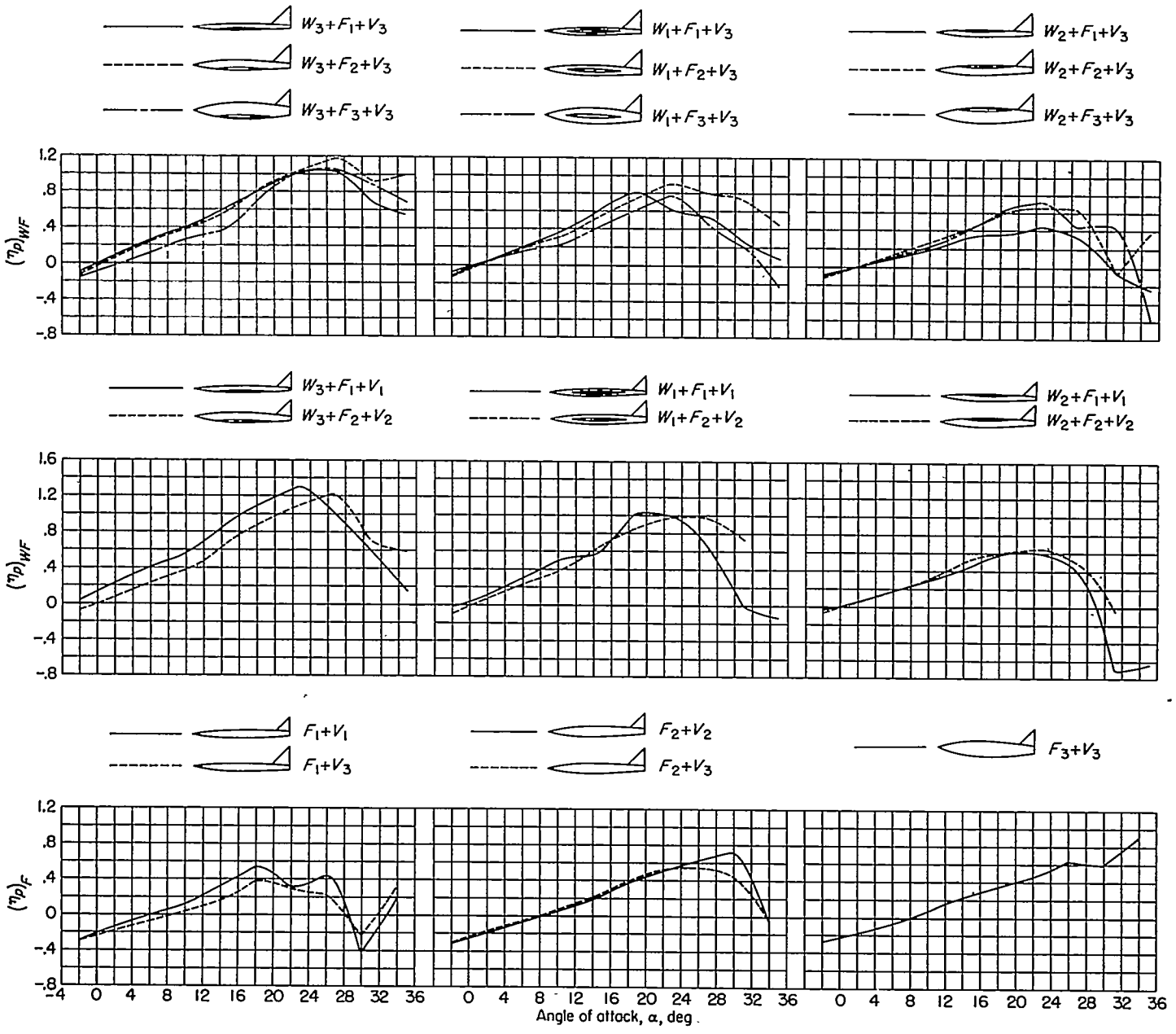

FIGURE 38.—Effects of wing position and fuselage size on the variation of the vertical-tail efficiency factors $(\eta_p)_{WF}$ and $(\eta_p)_F$ with angle of attack for several wing-fuselage-tail and fuselage-tail configurations.